AL.2.1989-9

CANADIANA
C2
NOV 16 1988

DEVELOPMENT AND PERFORMANCE EVALUATION OF AN ENERGY BUDGET SNOWMELT MODEL

RESEARCH MANAGEMENT DIVISION

Alberta Environment

Digitized by the Internet Archive
in 2016

https://archive.org/details/developmentperfo00gray

For more information on reports published by the Research Management Division, contact:

Alberta Environment
Public Communications Branch
12th Floor, Oxbridge Place
9820 - 106 Street
Edmonton, Alberta
T5K 2J6

Ph. 427-6267

This report may be cited as:

Gray, D.M. and P.G. Landine. 1988. Development and performance evaluation of an energy budget snowmelt model. Prep. for Alberta Environment, Research Management Division by Division of Hydrology, University of Saskatchewan. RMD Report L-113. 70 pp.

DEVELOPMENT AND PERFORMANCE EVALUATION
OF AN ENERGY BUDGET SNOWMELT MODEL

by

D.M. GRAY AND P.G. LANDINE

Division of Hydrology
University of Saskatchewan

for

RESEARCH MANAGEMENT DIVISION
Alberta Environment

RMD Report L-113

1988

The report is made available as a public service. The Department of Environment neither approves nor disagrees with the conclusions expressed herein, which is the responsibility of the authors.

EXECUTIVE SUMMARY

An Energy Budget Snowmelt Model (EBSM) that can be used in operational systems for forecasting streamflow from snowmelt in open grassland environments is developed and evaluated. Methods and procedures for estimating energy fluxes, albedo-depletion, and changes in the internal energy and water content of snowcover, from the extra terrestrial flux and atmospheric transmissivity and daily climatological observations of air temperature, relative humidity, snowfall, sunshine hours and wind speed are described.

The "starting" and "ending" dates of snowcover runoff predicted by the EBSM are compared with observations of snowcover depletion and "start" of streamflow from a small (10 km^2) and a large (350 km^2) watershed located near Regina, Saskatchewan. Reasonable agreement between the time elements of simulated and measured data is demonstrated. The need for a routine to account for the effects of storage on the translation and attenuation of melt quantities through a snowcover and in snow-filled gullies, especially in low snow years, is emphasized.

Simulated hydrographs generated with the U.S. Streamflow Synthesis and Reservoir Regulation system (SSARR) using: (a) the EBSM and (b) the temperature index model of the original system to calculate snowmelt are compared with observed streamflow. It is shown that the EBSM will provide information on streamflow of at least equivalent accuracy to that obtained with the "original" system and there is evidence to suggest that it may give improved estimates of the time-of-occurrence and rate of snowcover runoff over those obtained by a temperature-index model. The physical integrity and advantages of an energy balance approach in snowmelt calculations are stressed.

TABLE OF CONTENTS

Page

LIST OF TABLES x

LIST OF FIGURES xi

ABSTRACT xiii

1. PRAIRIE SNOWMELT MODEL 1
1.1 Introduction 1

2. ENERGY EQUATION 3

3. EVALUATION OF TERMS 4
3.1 Net Short-wave Radiation 4
3.1.1 Incoming Short-wave Radiation 4
3.1.2 Albedo 9
3.1.2.1 Premelt 11
3.1.2.2 Melt 11
3.1.2.3 Late-occurring snowcovers 13
3.2 Net Radiation 13
3.3 Net Long-wave Radiation; Premelt Period 16
3.4 Radiation Melt Model 22
3.4.1 Time of Melt 24
3.4.2 Albedo Model 25
3.4.3 Results and Discussion 29
3.5 Convective Energy Fluxes 36
3.5.1 Sensible Heat 37
3.5.2 Latent Energy 39
3.6 Ground Heat Flux 41
3.7 Heat Flux from Rain 41
3.8 Changes in Internal Energy 42

4. MODEL PERFORMANCE 47
4.1 Comparison Between "Start" and "Finish" of Snowcover Runoff and Decrease in Snow Depth 47
4.2 Comparison Between Start of Simulated and Observed Runoff 50
4.3 Streamflow Simulations 53
4.3.1 General 53
4.3.2 Implementation of EBSM in SSARR 54
4.3.2.1 Input Data 54
4.3.2.2 Basin processing routines 54
4.3.3 Creighton Tributary 55
4.3.4 Wascana Creek 60
4.3.5 Discussion 61

5. SUMMARY 65

6. REFERENCES CITED 68

LIST OF TABLES

Page

1. Julian day the net radiation flux turned positive and the albedo of shallow snowcovers ($d \lessapprox 25$ cm) started to deplete under different melt sequences. 26

2. Julian day the net radiation flux turned positive and the albedo of deep snowcovers ($d > 25$ cm) started to deplete under different melt sequences. 26

3. Effects of different input parameters on the mean and standard deviation of the difference between calculated (Q_{NC}) and measured (Q_{NM}) daily net radiation during Melt. 34

4. Comparison of daily estimates of sensible heat during snowmelt (MJ/m^2-d) by Eq. 23 with those calculated by detailed profile measurements. 38

5. Comparison of daily estimates of evaporation during snowmelt (mm/d) by Kuz'min's equation (Eq. 25) with those obtained from detailed profile measurements. 41

6. Julian day of "Start" and "End" of simulated snowcover runoff and decrease in measured snow depth at Bad Lake and Regina. 50

7. Julian day simulated snowcover runoff at Regina and observed streamflow on Davin and Wascana Creek watersheds started. 51

LIST OF FIGURES

Page

1. Relationship between measured daily short-wave radiation on days with $n/N > 0.9$ and the clear-sky flux calculated by Eqs. 6 and 7 with $p = 0.85$, Feb.-Apr., Bad Lake. 6

2. Relationships between daily short-wave radiation fluxes and sunshine ratio for different periods of the year and weather types at Bad Lake, Sask., 1972-1985 inclusive. 7

3. Schematic of the variation in the albedo of a Prairie snowcover with time during Premelt, Melt and Postmelt periods. 10

4. Albedo decay curves of Prairie snowcover during periods of continuous melt. 12

5. Relationship between daily net radiation and net short-wave radiation during Premelt, Melt and Postmelt periods. 15

6. Relationships between daily net radiation and net shortwave radiation. 17

7. Evaluation of coefficients of Brunt's equation. 20

8. Variation in the ratio of measured daily long-wave radiation ($Q_N - Q_s + Q_r$) to calculated fluxes with sunshine ratio n/N. 21

9. Relationships between measured daily net long-wave radiation ($Q_N + Q_r - Q_s$) and daily net long-wave radiation calculated by expressions given by (a) Brunt and (b) Satterlund. 23

10. Flow diagram of albedo model. 28

11. Measured and simulated albedo for a deep snowcover (>25 cm) and measured snowfall, net radiation and maximum air temperature plotted with time during Premelt, Melt and Postmelt periods - Bad Lake, Saskatchewan, 1974. 30

12. Measured and simulated albedo for a shallow snowcover ($\leq$25 cm) and measured snowfall, net radiation and maximum air temperature plotted with time during Premelt, Melt and Postmelt periods, Bad Lake, Saskatchewan, 1980. 31

continued ...

LIST OF FIGURES (CONCLUDED)

Page

13. Simulated versus measured albedo for 74 days of melt at Bad Lake, Saskatchewan, 1972-1982. 32

14. Comparison between calculated and measured net radiation for 67 days of melt, Bad Lake, Sask., 1972-1982. "Measured" net radiation used to establish "start-of-melt". 33

15. Comparison between calculated and measured net radiation for 67 days of melt, Bad Lake, Saskatchewan, 1972-1982. "Calculated" net radiation used to establish "start-of-melt". 35

16a. Flow diagram for internal energy accounting (Cont.) 44

16b. Flow diagram for internal energy accounting (Concld.) 45

17. Measured: albedo, snowdepth and snowfall and simulated: albedo and accumulated snowcover runoff for the Bad Lake climatological station plotted with time, Feb. 1 to Apr. 30, 1974. 48

18. Measured: albedo, snowdepth and snowfall and simulated: albedo and accumulated snowcover runoff for the Bad Lake climatological station plotted with time, Feb. 1 to Apr. 30, 1982. 48

19. Measured: albedo, snowdepth and snowfall and simulated: albedo and accumulated snowcover runoff for the Regina Airport plotted with time, Feb. 1 to Apr. 30, 1973. 49

20. Observed and simulated hydrographs from snowmelt; Creighton Tributary, 1974. 56

21. Observed and simulated hydrographs from snowmelt; Creighton Tributary, 1975. 57

22. Climatological data for Regina Airport and runoff hydrographs for Wascana Creek, 1982. 59

23. Simulated and observed hydrographs from snowmelt on Wascana Creek at Sedley for a low flow year, 1972. 62

24. Simulated and observed hydrographs from snowmelt on Wascana Creek at Sedley for a high flow year, 1974. 63

ABSTRACT

Meltwater released by the shallow snowcovers of the Canadian Prairies is an important water resource to the region. Therefore, many water management agencies are interested in methods of forecasting streamflow and seasonal water yield from snowmelt. Reliable, accurate forecasts require information of the time of melt and snowmelt rates and volumes. At the present time these quantities are usually estimated by simple temperature-index methods which have not proven successful in open grassland environments.

The report describes the development and testing of a snowmelt model which uses the energy equation as its' physical framework. Empirical procedures for evaluating radiative, convective, advective and internal energy terms from standard climatological measurements are presented. Algorithms for accounting for changes in the energy terms in a daily energy balance model are described.

The application of the energy budget snowmelt model (EBSM) for predicting ablation and simulating streamflow from small and large watersheds is evaluated. It is demonstrated that the EBSM in the U.S. Corps of Engineers Streamflow Synthesis and Reservoir Regulation model leads to general improvement in the performance of the system in synthesizing streamflow from Prairie snowmelt.

ACKNOWLEDGEMENTS

The writers wish to acknowledge the financial support provided to the project by the Water Research Support Program, Inland Waters Directorate, Environment Canada; the Natural Sciences and Engineering Research Council of Canada and the Research Management Division, Alberta Environment.

1. PRAIRIE SNOWMELT MODEL

1.1 INTRODUCTION

Snow is an important water resource in the semi-arid region of the Canadian Prairies. Although only approximately one-third of the annual precipitation occurs as snow, it produces 80% or more of the annual surface runoff. Meltwater derived from the shallow snowcover has many beneficial uses: as a domestic and livestock supply, as a wildlife habitat, for recharging soil water reserves, and other purposes; conversely, runoff may cause localized flooding, soil erosion and drainage problems. Thus, for different reasons, many agencies concerned with water management have interest in improved methods of predicting rates and volumes of snowmelt.

Knowledge of the time and amount of water released by snowmelt is essential for accurate short-term forecasts (1 day or 1 week) of flood flows, and reliable long-term forecasts of seasonal water yield and the soil moisture status at the time of seeding of annual crops. Numerous models have been developed for forecasting streamflow. One such model that has been used extensively by Environment Alberta for this purpose is the U.S. Corps of Engineers Streamflow Synthesis and Reservoir Regulation model (U.S. Army Corps of Engineers, 1972). However this model, like others, has been developed primarily from data collected in mountainous and forested terrain having deep snowpacks. Hence, its applicability for predicting discharge from Prairie watersheds may be questioned simply on consideration of differences in snowcover, topographic, climatic, vegetative and landuse factors between regions.

Phenomenologically, the conservation of energy is the basis of all snowmelt models. However, the relative importance to melt of the energy terms and transfer mechanisms varies widely with climate, vegetation, topography and other factors. For example, a forest canopy absorbs long-and short-wave radiation and emits long-wave radiation, thus controlling the net radiative exchange and the ambient air temperature at the underlying snow surface. Because the net long-wave exchange and the convective transfer of sensible energy are temperature dependent, temperature index methods for calculating snowmelt rates have proven successful in this environment. In open, grassland environments the amount of atmospheric radiation absorbed by a snowcover is governed principally by the intensity of the incident short-wave radiation flux and surface albedo; the net long-wave exchange process affects melt primarily by controlling the internal energy status of a snowcover. Meltwater is not released until the energy deficit of a snowcover is satisfied and it becomes isothermal at $0^{\circ}C$. Further, in open areas the relative magnitudes of net radiation and sensible heat, the fluxes which govern melt, can vary widely in time and snowcover conditions. For example, Granger et al. (1978) gives ratios for these fluxes of 0.33 and 2.67 on consecutive days of melt of a complete snowcover. Because solar radiation is often the dominant flux, particularly under complete snowcover, and the radiative and convective energy exchanges are poorly correlated, temperature index models of snowmelt tend to perform poorly in a prairie environment.

O'Neill (1972), Male and Gray (1975), Granger (1977), Granger et al. (1978) and Male and Granger (1979, 1981) have studied the energetics of melting prairie snowcovers. Their results suggest that because of the dynamical character of the energy terms, the small energy and mass storage capacities of the shallow snowcover, the short ablation period and other factors, reliable estimates of snowmelt are probable only if calculated within the physical framework of the energy equation applied to periods not longer than a day. In this report an energy balance snowmelt model which can be used for forecasting streamflow from shallow prairie snowcovers is developed and tested. To ensure that the model can be used on an operational basis, it includes procedures for estimating the energy terms from daily measurements of precipitation, sunshine hours, air temperature, relative humidity, and 10-m windspeed. The performance of the model in predicting snowcover ablation and streamflow is evaluated.

2. ENERGY EQUATION

The energy available for melting a unit volume of snowcover (Q_m) can be described by the equation:

$$Q_m = Q_{sn} + Q_{ln} + Q_h + Q_e + Q_g + Q_a - du/dt \qquad .1$$

where:

Q_{sn} = net short-wave radiation flux absorbed by the snowcover,

Q_{ln} = net long-wave radiation flux at the snow-air interface,

Q_h = convective sensible heat flux between the air and the snow surface,

Q_e = flux of latent energy (evaporation, sublimation, condensation) at the snow-air interface,

Q_g = flux of energy across the snow-ground interface by conduction,

Q_a = advective energy flux (rain, other external sources), and

du/dt = rate of change in internal (stored) energy per unit time.

The amount of melt can be calculated from Eq. 1 by the expression:

$$M = Q_m/(\rho h_f B) \qquad .2$$

where:

M = depth of snowmelt,

ρ = density of water,

h_f = latent heat of fusion, and

B = thermal quality of snow or the fraction of ice in a unit mass of wet snow.

For normal conditions, h_f = 333.5 kJ/kg and ρ = 1000 kg/m^3. Hence, Eq. 2 can be reduced to

$$M = Q_m/(3335\ B), \qquad .3$$

in which B is usually taken in the range 0.95-0.97. M is in cm when all other terms in Eq. 1 are in kJ/m^2.

3. EVALUATION OF TERMS

3.1 NET SHORT-WAVE RADIATION

The net short-wave radiation absorbed by a snow surface is equal to the difference between incoming (Q_s) and reflected (Q_r) fluxes, i.e. $Q_{sn} = Q_s - Q_r$. In most cases Q_r is taken as the product of Q_s and the surface albedo (A); hence net short-wave radiation is calculated as,

$$Q_{sn} = Q_s(1 - A). \qquad .4$$

3.1.1 Incoming Short-wave Radiation

Numerous investigators (Penman 1948; Mateer 1955; Brutsaert 1982) have shown that the daily short-wave radiation incident to the earth's surface (Q_s) can be related to the clear-sky insolation (Q_o) or the extra-terrestrial radiation flux (Q_A) and sunshine ratio (n/N) by expressions of the form:

$$Q_s = Q_o[a + b(n/N)], \text{ and} \qquad .5a$$

$$Q_s = Q_A[A + B(n/N)] \qquad .5b$$

in which a, A, b and B are empirically-derived coefficients whose magnitudes are evaluated from measured data. The sunshine ratio is the ratio of the actual number of hours of bright sunshine (n) to the maximum possible hours of sunshine, (N).

Short-wave radiation reaching the earth's surface has two components: a direct beam component along the sun's rays and a diffuse component scattered by the atmosphere. Direct clear-sky radiation falling on a slope (I_d) can be calculated by the procedure given by Garnier and Ohmura (1970) as:

$$I_d = (I_o/r^2)\int p^m \cos(X \wedge S)\,dH \qquad .6$$

where:

I_o = solar constant,

r = radius vector of the earth's orbit,

p = mean transmissivity of the earth's atmosphere,
m = optical air mass,
$\cos(X \wedge S)$ = cosine of the angle of incidence of the sun's rays on the slope. X is the unit normal vector pointing away from the surface and S is the unit vector expressing the sun's position, and
H = hour angle measured from solar noon. The integral is taken over the duration of sunlight on the slope.

Values of I_o, r and m are given by List (1968). The transmissivity (p) is largely a function of the water and dust content of the atmosphere and is highest in winter and lowest in summer. Gates (1980) has shown that p usually falls in the range 0.40 to 0.70 and where the air is clear, such as at high mountain elevations, $p = 0.80$. Recently, Mudiare (1985) suggested an average value for central Saskatchewan in the summer months of $p = 0.65$. For the snowmelt period in the European USSR, Kuz'min (1972) recommends a value of 0.80 ∓ 0.05.

The transmissivity may vary widely depending on season, elevation, latitude and other factors. An attempt was made to find an acceptable value for the "normal" snowmelt season on the Prairies by comparing daily short-wave fluxes, calculated by Eq. 6 with $p = 0.65$, 0.70, 0.75, 0.80 and 0.85, on days during Feb. to Apr. in which n/N was greater than 0.90, with corresponding values recorded by a Kipp solarimeter. The results of this analysis showed a transmissivity of 0.85 gave reasonable agreement in values (see Fig. 1); the mean difference is -0.822 MJ/m^2-d with a standard deviation of 1.57 MJ/m^2-d. It can be noted in Fig. 1 that the largest departures from the 45° line occur at the larger fluxes during the latter part of April and likely reflect the seasonal decrease in "p" toward the summer months.

All calculations of I_d reported in subsequent parts of this Section use $p = 0.85$.

A simple means of calculating the diffuse clear-sky radiation (D_o) is given by List (1968) as:

$$D_o = 0.5[(1-a_w-a_o)Q_A - I_d] \qquad .7$$

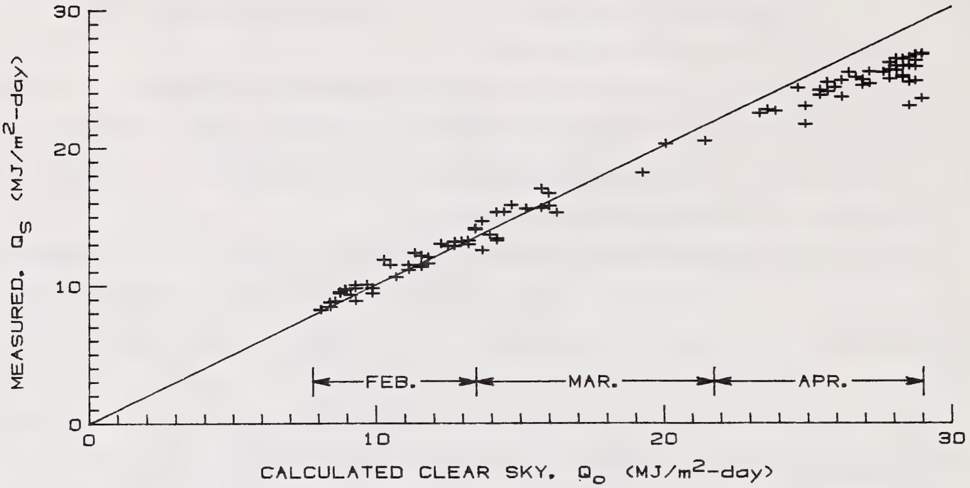

Figure 1. Relationship between measured daily short-wave radiation on days with n/N > 0.9 and the clear-sky flux calculated by Eqs. 6 and 7 with p = 0.85, Feb.-Apr., Bad Lake.

where:

a_w = radiation absorbed by water vapor (assumed to be 7%),

a_o = radiation absorbed by ozone (assumed to be 2%),

Q_A = extra-terrestrial radiation on a horizontal surface at the outer limit of the earth's atmosphere and equal to $(I_o/r^2)\int \cos z_s \, dH$, where z_s = sun's zenith distance (List, 1968), and

I_d = direct clear-sky radiation reaching the earth's surface.

The total short-wave, clear-sky flux incident to the earth's surface is the sum of direct beam and diffuse components, i.e. $Q_o = I_d + D_o$.

Figure 2 shows daily values of Q_s/Q_o and Q_s/Q_A plotted against n/N for Bad Lake during Feb-Apr. The "best-fit" regressions were calculated as:

$$Q_s/Q_o = 0.518 + 0.519 \text{ n/N} \quad \text{(clear sky), and} \qquad .8a$$

$$Q_s/Q_A = 0.404 + 0.421 \text{ n/N} \quad \text{(extra-terrestrial)} \qquad .8b$$

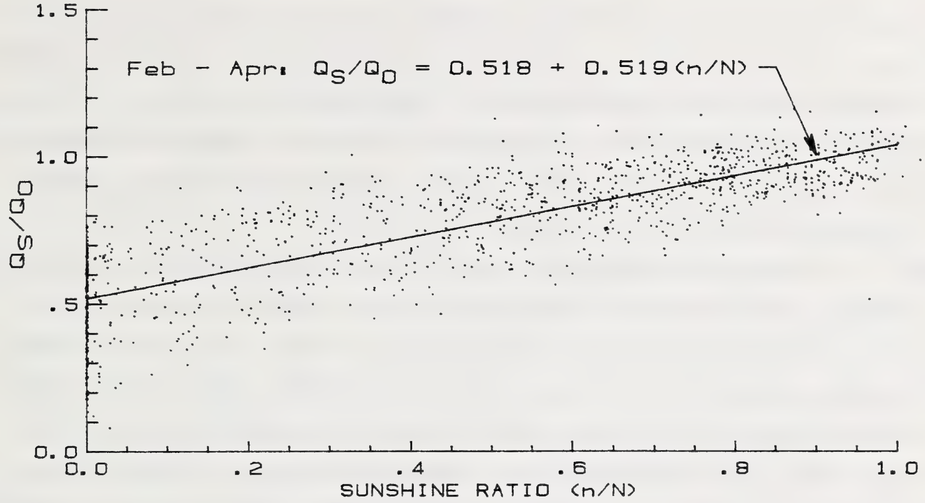

(a) CLEAR SKY

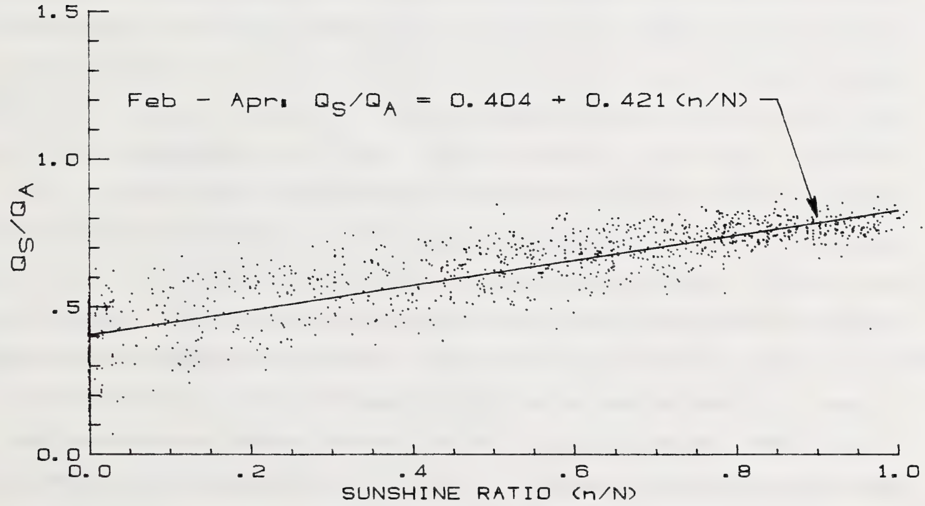

(b) EXTRA-TERRESTRIAL

Figure 2. Relationships between daily short-wave radiation fluxes and sunshine ratio for different periods of the year and weather types at Bad Lake, Sask., 1972-1985 inclusive: (a) Q_s/Q_o versus n/N; (b) Q_s/Q_A versus n/N. Q_s = measured flux; Q_o = calculated "clear-sky" flux; Q_A = extra-terrestrial flux and n/N = sunshine ratio.

Equation 8a has a correlation coefficient of 0.81 and a standard error of estimate of 0.12 whereas the corresponding values for Eq. 8b were 0.84 and 0.09, respectively. From these statistics it is evident that both equations have approximately the same predictive capability and it is believed that either would yield an estimate of Q_s of acceptable accuracy for practical use.

Equations 8a and 8b give the short-wave flux to a horizontal surface. Hence they must be adjusted for slope and aspect where these topographical facets are important to melt. In these regards the methods used to estimate clear-sky radiation separate the direct beam and diffuse components and I_d can be calculated directly by Eq. 6 for any slope. Male and Gray (1981) give graphs of the ratio of direct radiation received by a slope to that received by a horizontal surface for different latitudes and months.

There is always question about the transposibility of empirically-derived regressions, such as those described by Eqs. 8a and 8b, to a spatial scale because the coefficients are site specific. de Jong (1973) shows wide variation in A and B of Eq. 5b for daily, weekly and monthly observations during the growing season at 63 sites throughout the world. Interestingly, when the values calculated for the nine sites that measured daily observations are compared, the ranges of A and B are relatively small, for example A: 0.20 to 0.33, mean = 0.26; and B: 0.43 to 0.62, mean = 0.49. Similarly, Baier and Robertson (1965) reported little difference between the coefficients for the months of the growing season at Ottawa and Edmonton from year to year and used values of A = 0.251 and B = 0.616. More recently, Mudiare (1985) from analyses of 11 years of record at Bad Lake during the 4-month period May-August, showed that in general the coefficients for rain-free days differed significantly from those derived from data obtained on days with rain, however there was no trend for the magnitudes to change appreciably between months. He reported mean values of A = 0.27 and B = 0.47 for rainfree days and A = 0.20 and B = 0.56 for rain days. The above discussion lends a degree of support to the assumption that for operational purposes the relationships between Q_s, Q_A and n/N and Q_s, Q_o and n/N over a large part of the

Prairies, at least during the summer months, may be described by average values of A and B.

Within a region A and B can be expected to vary seasonally because of changes in climate and surface cover, hence in atmospheric optical properties and albedo. Over the Prairies, the transmissivity of the atmosphere for radiation is higher in winter than in summer due to a lower water and dust content and the low sun angle and high albedo of the snowcover can result in large reflected fluxes being back-scattered by clouds. For example, the transmissivities at Bad Lake during spring and summer periods were 0.85 and 0.65 respectively and the average values of A and B for the two periods were: Spring: A = 0.404 and B = 0.421 and Summer: A = 0.27 and B = 0.47. The larger ratio of Q_s/Q_A under complete cover (n/N = 0) in spring is attributed to both the higher transmissivity and increased contributions of back-scattered reflected radiation. The greater effect of increasing amounts of cloud cover in reducing Q_s in summer can be associated with changes in the physical properties of clouds, eg. water content, thickness, etc.

3.1.2 Albedo, A

The mean reflectance or albedo of a snowcover governs the amount of radiant energy absorbed and depends on grain size and density of the snow, the spectral composition and the direction (direct or diffuse) of the illuminating beam, sun angle, surface roughness, and other factors. For a shallow snowcover the surface of the ground may play a dominant role in the energy exchange because of reflection, absorption and re-radiation of short-wave radiation penetrating the snowcover. O'Neill (1972) suggests that the underlying ground can be expected to influence the apparent albedo of Prairie snowcovers when their depths are less than 4 to 6 cm.

A snowcover undergoes a natural decrease in its' albedo from the time of formation due to the process of metamorphism which affects its' optical properties. On the Prairies the decay in albedo can be accelerated by deposits of wind-transported soil or slowed by frequent small snowfalls. Normally, however, the largest change in albedo occurs during melt of the seasonal snowcover. It is in this period that the albedo-decay process must be accurately modelled in order to be successful in applying an energy balance for estimating snowmelt quantities.

Albedo decay curves for a melting Prairie snowcover were established from measurements of short-wave, incoming and reflected radiation. Previous comparisons between point measurements of albedo with aerial measurements, obtained using an inverted Kipp solarimeter mounted in an aircraft, showed reasonable agreement under both complete and patchy snowcover conditions (O'Neill 1972). These findings suggest that point measurements can be used as areal indices when snowcover conditions are reasonably similar, despite the fact that the latter is an integrated value for different topographical facets and land use (fallow, stubble, bush and lakes).

A review of point measurements for the months of Feb.-Apr., inclusive, showed that the change in albedo with time differred with snowcover and melt conditions. In general, the sequence could be separated to "Premelt", "Melt" and "Postmelt" periods as illustrated in Fig. 3.

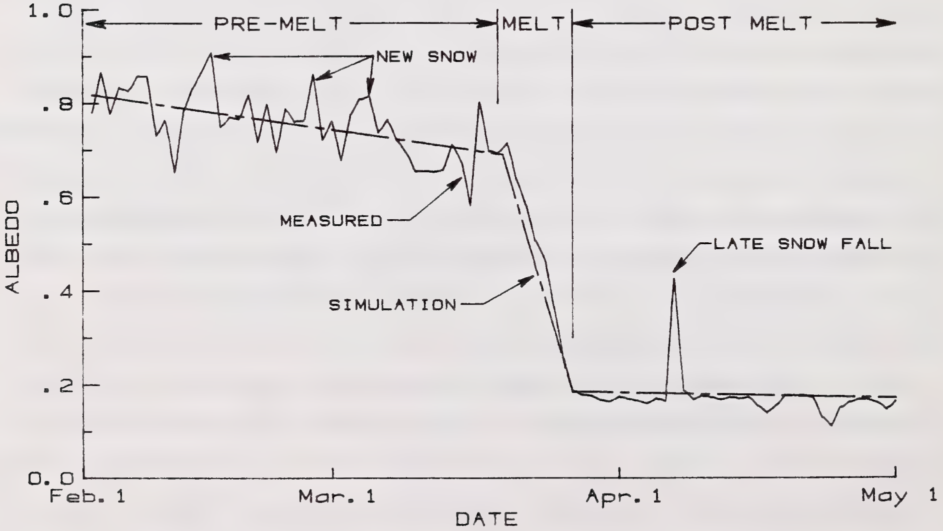

Figure 3. Schematic of the variation in the albedo of a Prairie snowcover with time during Premelt, Melt and Postmelt periods.

3.1.2.1 Premelt. "Premelt" is considered herein as the period extending from Feb. 1st of any year to the date melt leads to complete ablation and disappearance of the seasonal snowcover. During this time snowcover is usually fairly continuous and complete and except for the snowfall or melt events the albedo decreases slowly with time at a sensibly constant rate. Rates of decay in albedo were measured in the range 0.004 to 0.009/d with an average of 0.0061/d.

3.1.2.2 Melt. It is during this period the decrease in albedo is largest and most rapid. The decrease is brought about by changes in the optical properties of a snowcover caused by melt and meltwater percolation, the effects of the underlying ground surface on the energy exchange (eg. albedo), and the development of patchy snowcover conditions. Under continuous melt the albedo-decay curve takes on an "Ogee" or "S" shape and the shallow snowcover completely disappears in 4 to 7 days. The transition periods at the beginning and end of continuous depletion are usually short, spanning only 1 to 2 days; although as shown later the depth of snowcover appears to influence to some extent the length of transition at the beginning of melt.

Figure 4a shows albedo plotted with days of melt for seven years of point measurements at Bad Lake and four aerial flights (O'Neill 1971, 1972; Creighton, Saskatoon-Goose Lake) made in separate years along different lines in Saskatchewan. It can be observed that variations in the shape of the curves derived from point measurements in different years are as large as those in curves constructed from the aerial measurements. Also, the data indicate no apparent advantage in using an exponential function to describe depletion in albedo with time of melt over a linear model. The best-fit linear regression describing the relationship is:

$$A_s = 0.662 - 0.071t, \qquad .9$$

in which t is the number of days after the start of continuous, rapid depletion. The regression has a correlation coefficient of 0.81 and the slope of 0.071 is significantly different from 0 (< 1% probability).

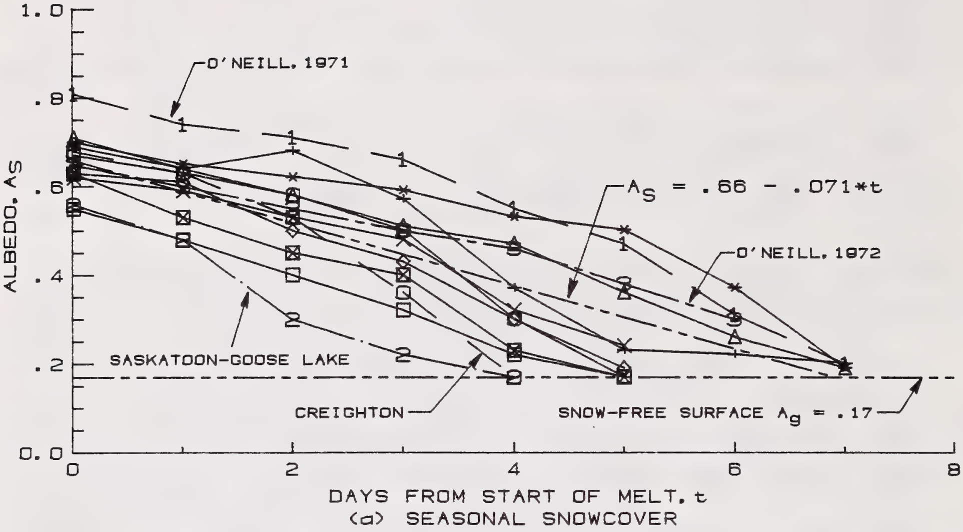

(a) SEASONAL SNOWCOVER

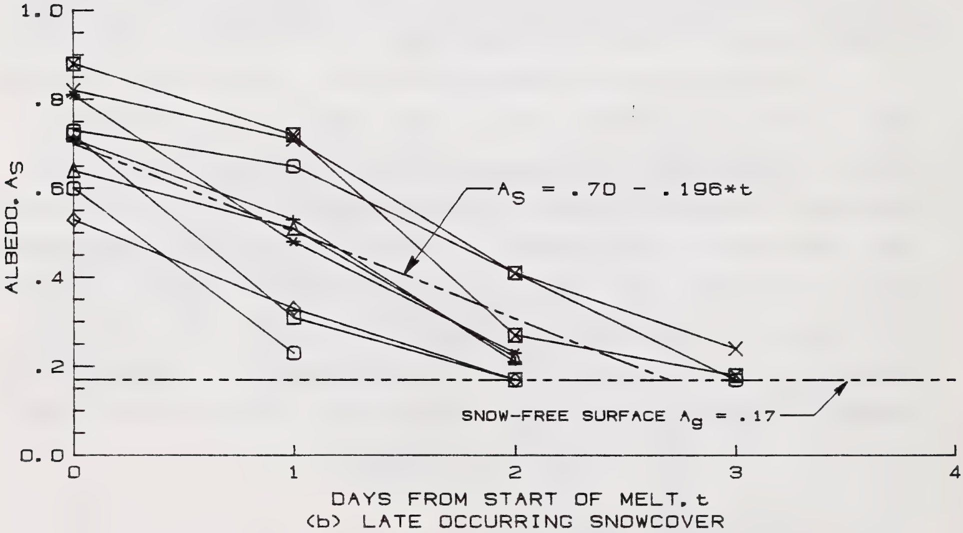

(b) LATE OCCURRING SNOWCOVER

Figure 4. Albedo decay curves of Prairie snowcover during periods of continuous melt: (a) seasonal snowcover and (b) late-occurring snowcover.

Because the relationship (Eq. 9) is linear and the albedo of the ground surface following the disappearance is reasonably constant (average $A_G = 0.17$), the albedo of the snowcover at the start of continuous melt establishes the duration of ablation. As shown in Fig. 4a, for the years of record the snowcovers disappeared in 4 to 7 days.

The results above have direct application in the development of a Prairie snowmelt model as they suggest the time variation in albedo can be described by three line segments: (1) Premelt - albedo decreases slowly at a rate of approximately 0.006/d; (2) Melt - albedo decreases at a rate of approximately 0.071/d and ablation usually occurs in a period of 4 to 7 days; and (3) Postmelt - the albedo of the snow-free ground surface may be taken equal to 0.17. These trends appeared to be relatively independent of the time of occurrence of major melt, that is Feb., Mar. or early Apr.

3.1.2.3 Late-occurring snowcovers. Frequently on the Prairies storms producing snowfall occur after the disappearance of the seasonal snowcover. The albedo of these snowcovers usually differs from that of the seasonal snowcover because of differences in the physical properties of the snow such as crystal size and shape, density, wetness, degree of contamination and other factors. Also, because they usually occur later in the spring when the short-wave flux is large they ablate rapidly. Figure 4b shows the change in albedo with days of melt for late-occurring snowcovers. It is evident that disappearance usually occurs within 2 to 4 days of the start of active melt. The best-fit equation was calculated as:

$$A_s = 0.70 - 0.196t \quad .10$$

3.2 NET RADIATION

Net radiation is the sum of the net short-wave flux absorbed by the snowcover (Q_{sn}) and the net long-wave flux at the surface (Q_{ln}), i.e.

$$Q_N = Q_{sn} + Q_{ln} \quad \text{or,} \quad .11a$$

$$Q_N = Q_s(1-A_s) + Q_{ln} \qquad .11b$$

Q_{ln}, the difference between the long-wave radiation emitted downward from the atmosphere and the flux emitted upward by the snow surface, is affected by many factors. The emissivity, temperature and absorptivity of the snow and atmosphere, the "field-of-view" of the emitting surface, the vapor pressure of the atmosphere, cloud cover, and others. Hence calculation of the term from theoretical considerations is usually cumbersome, requires measurements of a number of variables, and often leads to tenuous results. For these reasons, and in attempt to keep the snowmelt model simple, an investigation was undertaken to determine the relative importance of the net long-wave flux to the radiative balance of a shallow Prairie snowcover.

Davies (1965, 1967) and Davies and Idso (1979) have demonstrated from analyses of both daytime and daily values of net radiation that over bare, vegetative surfaces Q_{sn} is the dominant flux and plots of Q_N and Q_s are remarkably linear with high correlation coefficients. The studies suggest that variations in albedo over vegetative surfaces during the summer months are small and do not vary widely under clear sky conditions. Further, Davies and Buttimor (1969) noted that the linear association could also be applied to sky conditions when the incoming long-wave radiation is not constant.

Daily values of Q_N were plotted against the net short-wave flux, taken as the difference Q_s-Q_r using data reported at Bad Lake for Feb. through Apr. (see Fig. 5). Figure 5 shows a strong linear trend between Q_N and Q_{sn} and the equation of the best-fit line was determined as:

$$Q_N = -2.15 + 0.630\ Q_{sn} \qquad .12$$

in which Q_N and Q_{sn} are in MJ/m^2-day. The relationship has a correlation coefficient of 0.92 and a standard error of estimate of 1.65 MJ/m^2-day. The high correlation coefficient is surprising inasmuch as Q_{sn} was calculated as the difference between incoming and reflected short-wave radiation measured by two sensors which would tend to

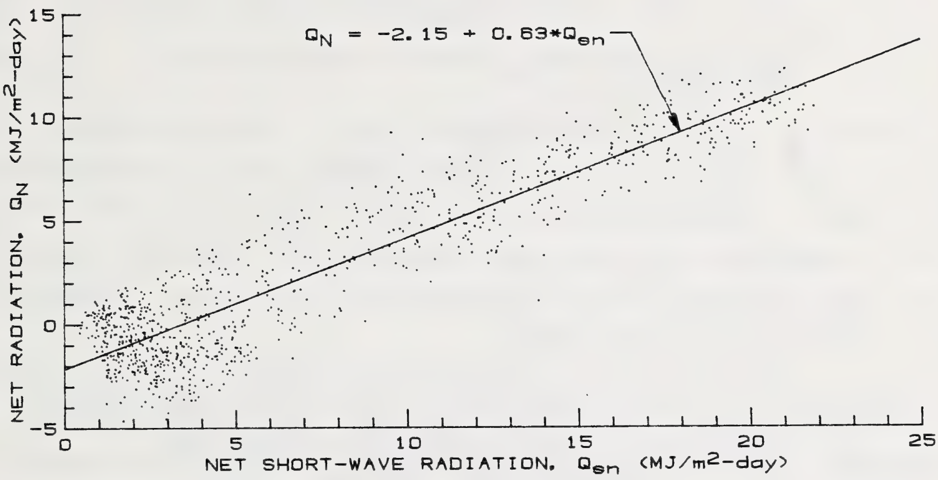

Figure 5. Relationship between daily net radiation and net short-wave radiation during Premelt, Melt and Postmelt periods.

induce errors in the term. Also, the data include days with complete snowcover, melting snowcovers, and bare ground; that is they represent a range of surface conditions over which Q_{ln} would be expected to change. Nevertheless, based on the result one would conclude that Q_{sn} is the dominant flux affecting Q_N (see discussion below).

The data were stratified to two periods; (a) Premelt - complete, non-melting snowcover and (b) Melt and Postmelt -continuous melt and a snowfree ground. The grouping of points for Melt and Postmelt periods was accepted because the regressions of Q_N and Q_{sn} for the two periods did not differ significantly. Figure 6a shows that in these periods Q_N and Q_{sn} are related by the equation,

$$Q_N = -0.371 + 0.522Q_{sn} \quad , \qquad .13$$

which has a correlation coefficient of 0.89 and a standard error of estimate of 1.39 MJ/m^2-d.

Equations 8a and 8b were combined with Eq. 13 and the calculated values of Q_N were regressed against their corresponding measured values. This analyses led to the empirical relationships:

$$Q_N = -0.526 + 0.465Q_o[0.518 + 0.519(n/N)](1-A), \text{ and} \qquad .14a$$

$$Q_N = -0.547 + 0.485Q_A[0.404 + 0.421(n/N)](1-A). \qquad .14b$$

in which Q_N, Q_o and Q_A are in MJ/m^2-d (Fig. 6). Equation 14a has a correlation coefficient $r = 0.87$ and a standard error of estimate s_E = 1.55 MJ/m^2; the corresponding values for Eq. 14b were $r = 0.87$ and s_E = 1.57 MJ/m^2-d. It is considered that either Eq. 14a or Eq. 14b would provide an estimate of Q_N of acceptable accuracy for use in a practical, operational snowmelt model.

Figure 6b shows a poor association between Q_N and Q_{sn} during the Premelt period; the association between the variables has a correlation coefficient of 0.08. The findings provide strong evidence that during Premelt the net long-wave flux is the dominant term influencing Q_N. This conclusion is supported by the large number of negative values of Q_N.

It is well known that during winter and in early spring the internal energy content of a Prairie snowcover can undergo wide diurnal cycling due to large nocturnal long-wave radiation losses. The net long-wave radiation exchange during Premelt is therefore extremely important in a Prairie snowmelt model as it directly affects the time and release pattern of snowcover runoff.

3.3 NET LONG-WAVE RADIATION; PREMELT PERIOD

The net long-wave flux is composed of downward radiation emitted by the atmosphere ($L\downarrow$) and the upward flux emitted by the surface ($L\uparrow$). During winter over snow, $L\uparrow$ is usually greater than $L\downarrow$ so that there is a net loss of energy from the snowpack.

$L\downarrow$ is emitted by ozone, carbon dioxide and water vapor from all atmospheric levels; under clear skies the largest portion originates within 100 m of the ground. Most of the long-wave radiation originates from water vapor and variations in $L\downarrow$ are largely due to variations in the amount and temperature of the water vapor. Hence, many investigators have found reasonable correlations between $L\downarrow$ and

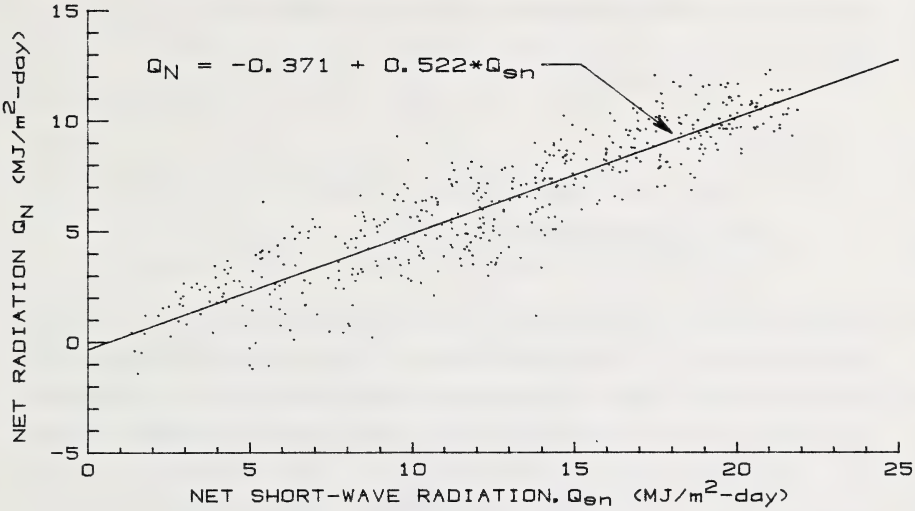

(a) MELT AND POST MELT

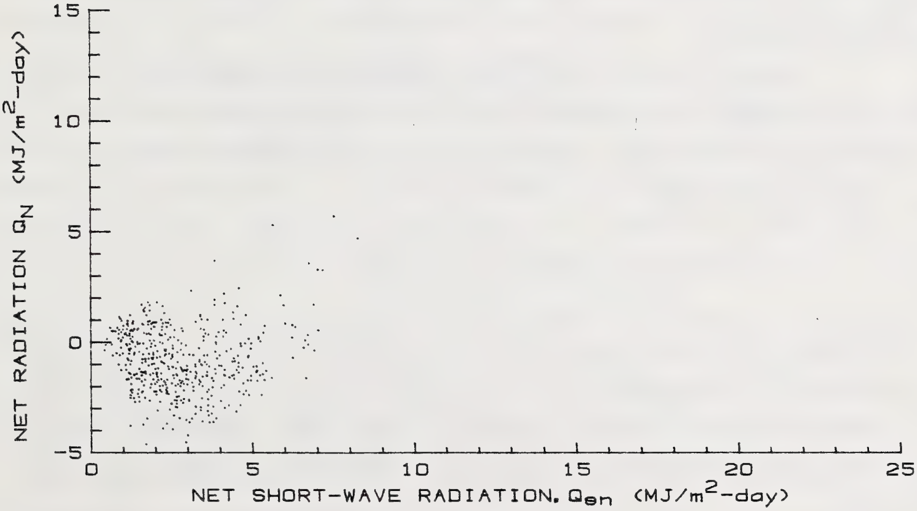

(b) PRE-MELT

Figure 6. Relationships between daily net radiation and net short-wave radiation: (a) Melt and Postmelt and (b) Premelt.

air temperature and vapor pressure. The most widely quoted of these relationships was first suggested by Brunt (1932):

$$L\downarrow = \sigma T_a^2(a + b\sqrt{e_a}) \qquad .15$$

where:

σ = Stefan-Boltzman constant ($4.899{*}10^{-9}$ MJ/m^2-d),

T_a = air temperature ($^{\circ}$K), and

e_a = actual vapor pressure of the air (mb or kPa).

Direct comparisons of Brunt's equation with measured data collected over snow are scarce. Male and Granger (1979) compared measured values of L↓ with values calculated with the mean daily air temperature and vapor pressure for clear days over a melting Prairie snowcover and concluded that Brunt's formula is a poor estimator of L↓. They attributed the poor correlation to fog, haze, or ice crystals commonly present at night in the air above a snowcover which experiences melting during the day. However no data are provided with respect to the applicability of Eq. 15 for estimating L↓ over non-melting surfaces.

Recently Satterlund (1979) suggested an empirical relationship for estimating L↓ based on the screen temperature and screen vapor pressure which gave good results at low temperatures. His equation has the form:

$$L\downarrow = 1.08\sigma T_a^4[1 - \exp(-e_a^{(T_a/2016)}] \qquad .16$$

in which T_a is in $^{\circ}$K and e_a is in mb. The performance of Eq. 16, when compared with other methods of calculating L↓ at temperatures below 0°C, suggests that it may be useful for modelling the long-wave incoming energy to the surface of a Prairie snowcover during the premelt period.

The long-wave radiation emitted by a snow surface (L↑) is usually calculated on the assumption that snow is a near-perfect black body in the long-wave portion of the spectrum. Thus,

$$L\uparrow = \varepsilon_s \sigma T_s^4, \qquad .17$$

where T_s is the absolute temperature of the snow surface (K) and ε_s is the emissivity which takes on values between 0.97 and 1.0.

Combining Eqs. 15 and 16 with Eq. 17 gives expressions for the net long-wave radiation flux as:

$$Q_{ln} = \sigma T_a^4 (a + b\sqrt{e_a}) - 0.97\sigma T_s^4 \text{, and} \qquad .18a$$

$$Q_{ln} = 1.08\sigma T_a^4 [1 - \exp(-e_a^{T_a/2016})] - 0.97\sigma T_s^4 \ . \qquad .18b$$

The coefficients for the Brunt equation were calculated by regressing $\{[(Q_N - Q_s + Q_r)/\sigma T_a^4] + 0.97\}$ against $\sqrt{e_a}$ on clear days ($n/N > 0.9$) over non-melting snowcovers. Also, it was assumed $T_s \simeq T_a$. The best-fit equation was calculated as

$$Q_{ln} = \sigma T_a^4 (0.58 + 0.094\sqrt{e_a}) - 0.97\sigma T_a^4 \ , \qquad .18c$$

and is shown plotted in Fig. 7. Interestingly, although the association is not strong, $r = 0.65$, the magnitudes of the coefficients; $a = 0.58$ and $b = 0.094$ are within the range of values reported by many other investigators (see Kondratyev 1969).

Equations 18b and 18c give an estimate of clear-sky Q_{ln} and thus they must be adjusted for cloud cover. Unfortunately, measurements of the character of clouds and degree of cloudiness are not recorded at the station and the weakness in the use of the sunshine ratio to index cloudiness in a relationship for net long-wave radiation is recognized. It is during the nocturnal hours that the long-wave exchange is most intense and only on days when cloud conditions are similar during day and night can n/N be expected to provide a satisfactory index. Despite the problems, in an effort to gain a first-approximation of Q_{ln} on cloudy days, the ratios of values of Q_{ln} determined from a radiation balance, i.e. $Q_{ln} = Q_N - Q_s + Q_r$ and the corresponding values calculated by Eqs. 18b and 18c with $T_s = T_a$ were regressed against the sunshine ratio and this led to the expressions:

$$\frac{Q_{ln}(\text{measured})}{Q_{ln}(\text{Brunt})} = 0.261 + 0.808(n/N) \text{, and} \qquad .19a$$

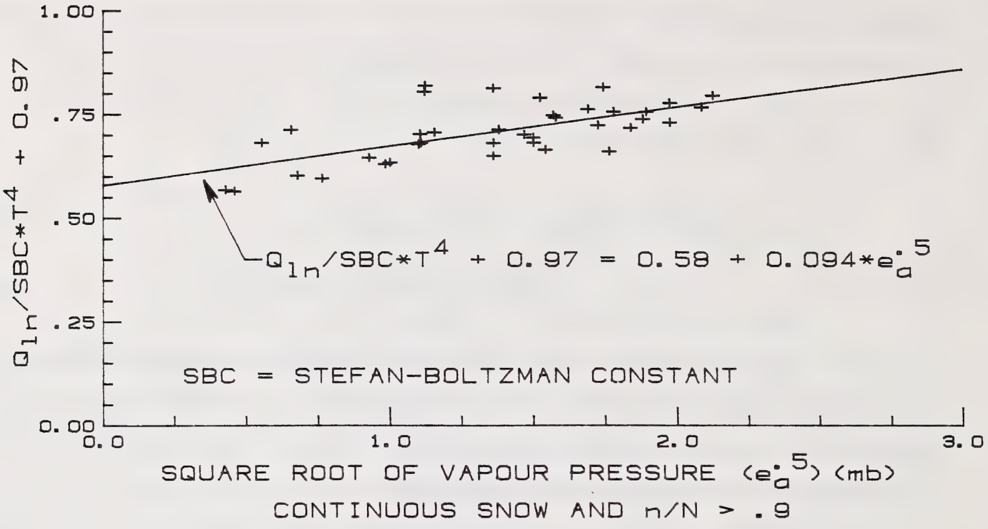

Figure 7. Evaluation of coefficients of Brunt's equation (Eq. 15) based on the relationship $\{(Q_N - Q_S + Q_r)\sigma T_a^4\} - 0.97$ and $\sqrt{e_a}$ for clear days over a non melting snowcover.

$$\frac{Q_{ln}(\text{measured})}{Q_{ln}(\text{Satterlund})} = 0.245 + 0.828(n/N). \qquad .19b$$

These data are plotted in Fig. 8. Each regression is highly significant (< 1% probability) and they clearly demonstrate that cloud cover is an important parameter affecting the net long-wave exchange during Premelt. Equation 19a (Brunt) gave a correlation r = 0.81 and Eq. 19b (Satterlund) an r-value equal to 0.84.

Based on the best-fit coefficients of Eqs. 18b, 18c, 19a and 19b, two empirical equations which may be used to estimate Q_{ln} for a Prairie snowcover were derived. These take the form:

$$Q_{ln} = -0.085 + 0.965\{\sigma T_a^4(-0.39 + 0.0934\sqrt{e_a})$$

$$\times [0.261 + 0.808(n/N)]\} \qquad .20a$$

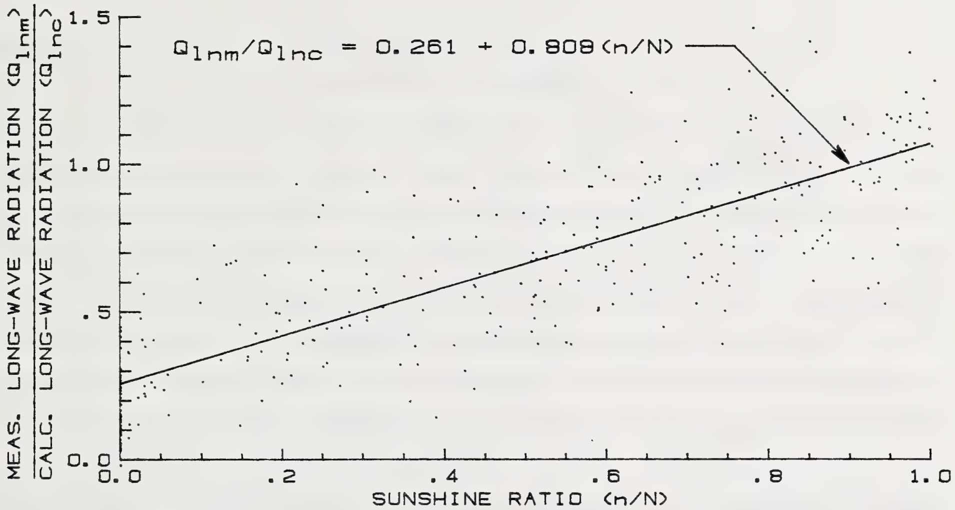

(a) BRUNT

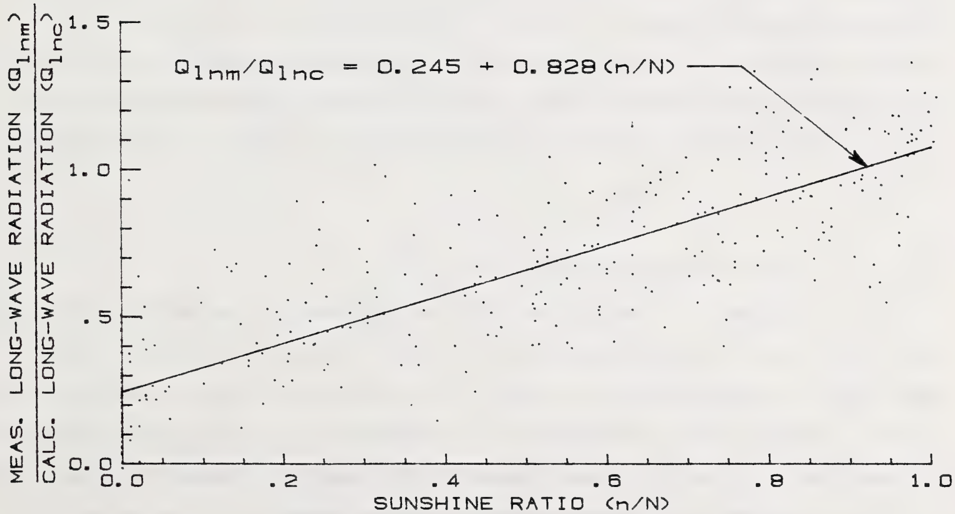

(b) SATTERLUND

Figure 8. Variation in the ratio of measured daily long-wave radiation $(Q_N - Q_s + Q_r)$ to calculated fluxes with sunshine ratio n/N: (a) Brunt, (b) Satterlund.

$$Q_{ln} = -0.031 + 0.974\{\sigma T_a^4[1.08(1-\exp(-e_a^{T_a/2016}))-0.97]$$

$$\times\ [0.245 + 0.828(n/N)]\} \qquad .20b$$

in which Q_{ln} is in MJ/m^2-d; $\sigma = 4.899{*}10^{-9}$ MJ/m^2-d; e_a is in mb and T_a in ^{o}K. Eq. 20a has a correlation coefficient, r = 0.82 and a standard error of estimate, s_E = 1.09 MJ/m^2-d; the corresponding values for Eq. 20b are r = 0.83 and s_E = 1.07 MJ/m^2-d. From these statistics it is evident that the relations have approximately equal predictive capability. Whether these estimates are acceptable for a snowmelt model remains to be evaluated, for example by the sensitivity of the quantity of melt or the time of occurrence of snowcover runoff to changes in Q_{ln}. As stated before, the correlations may be improved by using a better indices of cloudiness and nocturnal cloud cover. Also, procedures need to be developed for estimating the snow surface temperature. Dybvig (1977) reported a high correlation between T_a, measured 20 cm above a snowcover, and T_s, measured at a depth of 1 cm in the snow. The association between T_a and T_s can be expected to decrease with increasing height of measurement of T_a. Figures 9a and 9b show daily radiative-balance values of Q_{ln} plotted against the corresponding values from Eq. 20a (Brunt) and Eq. 20b (Satterlund) for the Premelt Period.

3.4 RADIATION MELT MODEL

Either Eq. 14a or Eq. 14b can be used to calculate the daily net radiative flux during periods of melt from the clear-sky insolation (Q_o) or extraterrestrial (Q_A) flux, sunshine ratio (n/N) and the surface albedo (A). Procedures for estimating Q_o and Q_A are detailed in Section 3.1.1 and the maximum possible number of sunshine hours (N) is fixed in time and space. Assuming measurements of the actual number of sunshine hours (n) are available, the expressions require an estimate of surface albedo.

In Section 3.1.2 the albedo-depletion characteristics of shallow prairie snowcovers were discussed. It was proposed that in years of infrequent midwinter melt events, the depletion in the period

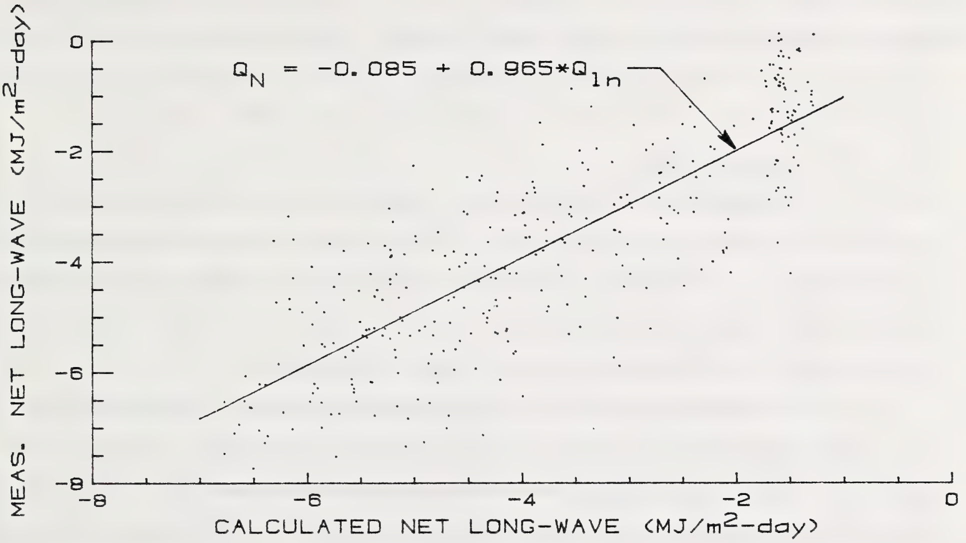

a) BRUNT

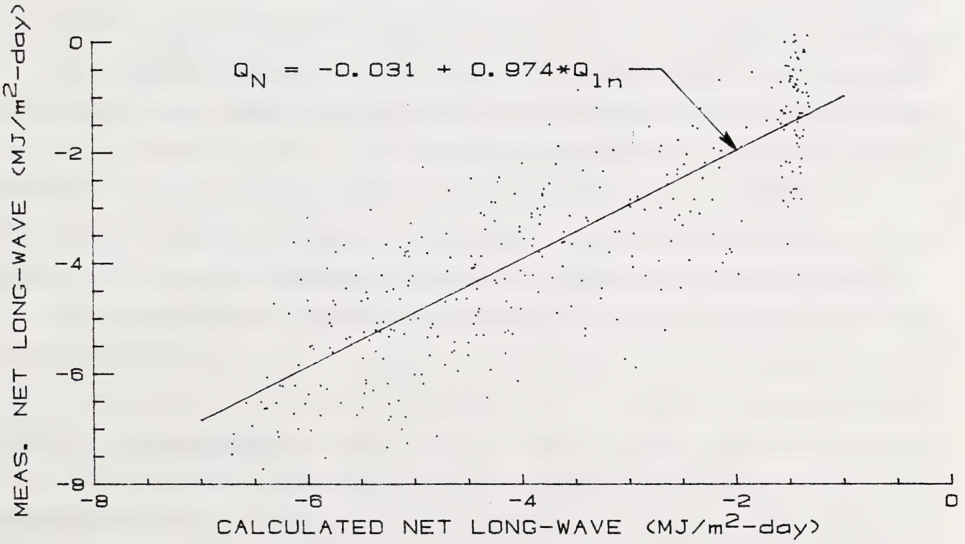

b) SATTERLUND

Figure 9. Relationships between measured daily net long-wave radiation ($Q_N + Q_r - Q_s$) and daily net long-wave radiation calculated by expressions given by: (a) Brunt and (b) Satterlund.

from late winter to disappearance of the seasonal snowcover could be approximated by three line segments of different slope encompassing the periods of Premelt, Melt and Postmelt. These general trends form the basis of a "Prairie" albedo model.

3.4.1 Time of Melt

Implementation of the model requires an initial value for albedo in late winter (e.g. Feb. 1st), which in the absence of new snow, usually falls in the range of 0.60 - 0.70 (average equal to 0.66). Note, the disappearance of a snowcover is fixed by the day the albedo takes on the value for the ground surface.

To establish the start of the Melt period it was assumed that the initiation of melt could be indexed by the day the net radiation flux became positive and remained positive for several days. In years with extended periods of cold weather and complete snowcover the daily net radiation flux during Premelt is usually negative or takes on small positive values (see Fig. 6b). The poor association of Q_N and Q_{sn} shown in the figure is due to the small fluxes of global radiation and large, nocturnal long-wave losses. During Melt and Postmelt the two variables show a strong association (correlation coefficient equal to 0.91) (Fig. 6a).

Tables 1 and 2 list the Julian day the net radiative flux (Q_N) turned positive and the corresponding day the albedo (A) started to deplete during continuous and interrupted melt sequences over 11 years of record. The data in Table 1 are for shallow snowcovers (initial depth $\leq$ 25 cm) and those in Table 2 for deep snowcovers (initial depth > 25 cm). Note, the snow depth is the mean calculated from observations made on a snow course located adjacent to the radiometers. The selection of 25 cm to differentiate shallow and deep snowcovers was arbitrary and based on visual observations of differences in the shapes of the snowcover and albedo depletion curves near the start of melt. In deep snowcovers the rate of decrease in albedo increased slightly during the "transition" from "Premelt" to "Melt" to an average value of 0.015/d and the occurrence of accelerated, rapid, depletion was delayed until the snowcover depth was about 25 cm and the albedo had decreased to approximately 0.65. The findings are consistent with data reported by Kuz'min (1972) which show a slower decrease in albedo per unit decrease in depth occurring prior to rapid, continuous ablation in snowcovers deeper than 30 to 40 cm.

Table 1 shows agreement between the start of depletion in A of shallow snowcovers, and the occurrence of a positive Q_N within -1 to +4 days; if 1976 were excluded the agreement would be within three days. These findings suggest that in most years Q_N can be used to index the day a shallow snowcover begins "active" melt. Exceptions to this general rule are years in which the positive fluxes of Q_N are small and the mean ambient air temperature is significantly above or below freezing. Such a case occurred in 1984 when the decrease in albedo lagged the positive flux of Q_N by 5 days because the daily maximum air temperatures during the period were 0° C or below, with lows reaching -14° C. At these temperatures the sensible energy flux and the internal energy content of the snowcover would take on large negative values. The finding is important as it points to the need for including a "threshold" air temperature in the modelling scheme.

Table 2 lists data for deep snowcovers (> 25 cm) and it is evident that the range in the differences between the times of occurrence of a decrease in A and a positive Q_N are much larger than for shallow snowcovers. They range from -6 to +6 days. Although the exact physical explanation for the wider range can not be given, it is attributed to the integrated effects of depth on snowcover optical properties, energetics, water storage characteristics, compressibility and other factors.

3.4.2 Albedo Model

An albedo model was developed on the findings detailed above. Figure 10 is a schematic flow diagram of the routine. A_t, $A_{(t-1)}$ = snowcover albedo on day t and day (t-1) respectively; DR = daily albedo decay (depletion) rate (1/d); MT = threshold melt temperature ($^\circ$C); Q_N = daily net radiation (MJ/m^2-d); TMIN, TMAX = minimum and maximum daily air temperatures ($^\circ$C); d = depth of snowcover (cm); SF = daily snowfall (cm); and WINTER = a logical variable which becomes

Table 1. Julian day the net radiation flux turned positive and the albedo of shallow snowcovers ($d \lesssim 25$ cm) started to deplete under different melt sequences.

Year	Melt Sequence[a]	Day Net Radiation Turned Positive and Depletion Began		Snow Depth
		Q_N	Albedo (A)	cm
1973	I	53	52	14
1976	C	89	93	8
1977	C	65	64	6
1979	I	65	64	16
	C	74	73	8
1981	C	47	47	9
1982	C	99	99	12
1983	I	43	42	13

[a] Melt Sequence: C = continuous melt which led to disappearance of the snowcover; I = depletion was interrupted, snowcover did not ablate completely and Q_N became negative during ablation.

Table 2. Julian day the net radiation flux turned positive and the albedo of deep snowcovers ($d > 25$ cm) started to deplete under different melt sequences.

Year	Melt Sequence[a]	Day Net Radiation Turned Positive and Depletion Began		Snow Depth
		Q_N	Albedo (A)	cm
1972	C	76	70	38
			80[b]	28
1974	I	85	88	46
	C	98	104	26
1975	C	101	101	36
			107[b]	27
1978	C	81	79	26

[a] Melt Sequence: C = continuous melt which led to disappearance of the snowcover; I = depletion was interrupted, snowcover did not ablate completely and Q_N became negative during ablation.

[b] Day when albedo began rapid, accelerated depletion.

false when A_t reduces to a value of 0.17. WINTER is re-instated on any day when TMAX falls below -6° C and Q_N is less than 1 MJ/m^2-d. The threshold temperature is obtained by the expression:

$$MT = -0.064 \text{ Dayno} + 6.69 \ . \qquad .21$$

in which MT is in $^{\circ}C$ and Dayno is the Julian day number. Equation 21 is based on the work of McKay (1964) who found that the daily mean temperature above 0° C which produced melt (ablation) by the temperature index method decreased with Dayno. This is attributed to the higher "negative" internal energy content (cold content) of the shallow snowcover during the winter months.

A brief description of the algorithm follows (refer to Fig. 10). Initially the depth of snowcover is checked and if greater than 25 cm with an albedo > 0.65 the depletion rate is set at 0.015/d (deep snowcover). It then checks for new snow and if the accumulation is greater than 0.5 cm the albedo is increased by the factor 0.1 SF. This adjustment was arrived at after review of the changes in simulated albedo caused by new snowfall. The model questions whether it is WINTER. If no, the albedo is reduced by 0.2, the daily depletion for a late-occurring snow (Postmelt period); if yes, the albedo of the newly-fallen snow is decreased by 0.05 for the first two days following the occurrence. This is an average depletion rate for midwinter snows. Three criteria are then interrogated to decide melt, namely, TMIN $> -4^{\circ}$ C; TMAX $\geq 0^{\circ}$ C and $Q_N > 1.0$ MJ/m^2; and $Q_N > -0.5$ MJ/m^2 and TMAX > MT. These combinations of Q_N, TMIN and TMAX which decide melt were obtained by trial and error and they index combinations of the energy fluxes, i.e. net radiation and convective energy, that produce melt. If any condition is satisfied, melt is assumed to occur and the albedo is reduced by 0.071, the rate for the Melt Period. Conversely, if no condition is satisfied, the albedo is assumed to decrease at the Premelt rate of 0.006/d.

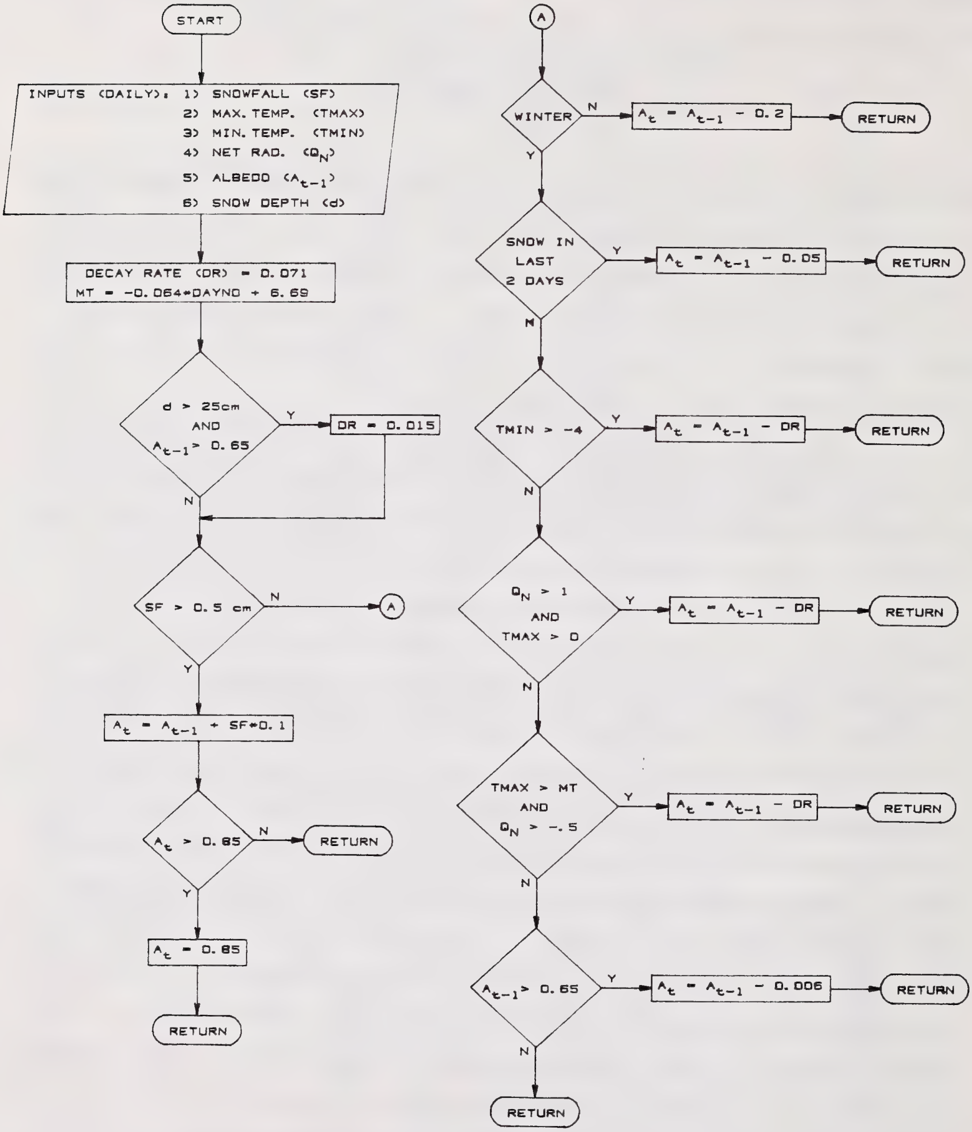

Figure 10. Flow diagram of albedo model.

3.4.3 Results and Discussion

Figures 11 and 12 show measured and simulated albedo and measured snowfall, maximum air temperature and net radiation plotted with time from Feb. 1st to Apr. 30th for 1974 and 1980. The data for 1974 (Fig. 11) are for a "deep" snowcover (snow depth approximately 46 cm at the start of Melt) whereas those for 1980 (Fig. 12) are for a "shallow" snowcover with a depth of about 9 cm. In each year the measured and simulated albedo-depletion curves are in relatively close agreement. For hydrological purposes, especially when used to calculate maximum snowmelt rates, the critical time the model must produce good estimates of albedo is during Melt. Figure 13 shows simulated albedo (A_s) plotted against measured albedo (A_m) for 74 days of melt. The mean of the difference (A_s - A_m) is -0.0007 with a standard deviation in individual values of 0.17. It is interesting to note the vertical and horizontal concentrations of data around the coordinate 0.17, 0.17. The vertical distribution of points represents cases where the snow under the solarimeter disappeared earlier than predicted by the model; the points distributed in the horizontal direction represent cases when the model simulated the albedo of bare ground in advance of the measurements. In most cases the dispersion about the 45^o line can be attributed primarily to errors in estimating the time of melt. Because the values of the mean difference and standard deviation are small, it is suggested that the model will provide estimates of albedo of acceptable accuracy for practical use.

To demonstrate the use of the model in calculating daily net radiation, comparisons were made between calculated and measured fluxes for 67 days of melt (see Fig. 14). The mean difference between calculated (Q_{NC}) and measured (Q_{NM}) net radiation was 0.49 MJ/m^2 with a standard deviation of the difference equal to 2.05 MJ/m^2. The offset in the mean difference (0.49 MJ/m^2) is primarily the result of calculations for 1972 when the albedo depletion simulated by the model occurred before the measured decrease. If the data for this year are excluded the mean difference is -0.13 MJ/m^2. Part of the variance of the differences can also be attributed to inaccuracies in the measurement of net radiation. During Melt the ambient humidity over a

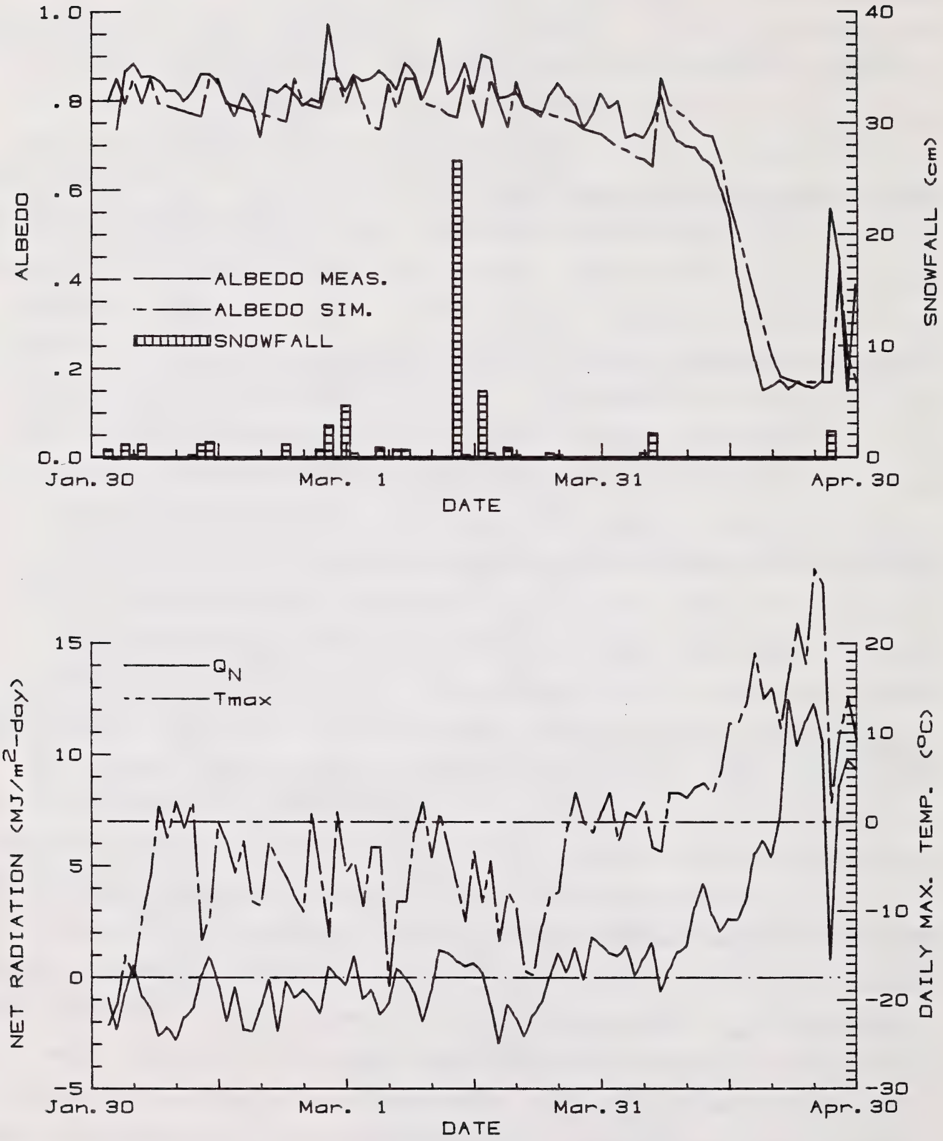

Figure 11. Measured and simulated albedo for a deep snowcover (>25 cm) and measured snowfall, net radiation and maximum air temperature plotted with time during Premelt, Melt and Postmelt periods - Bad Lake, Saskatchewan, 1974.

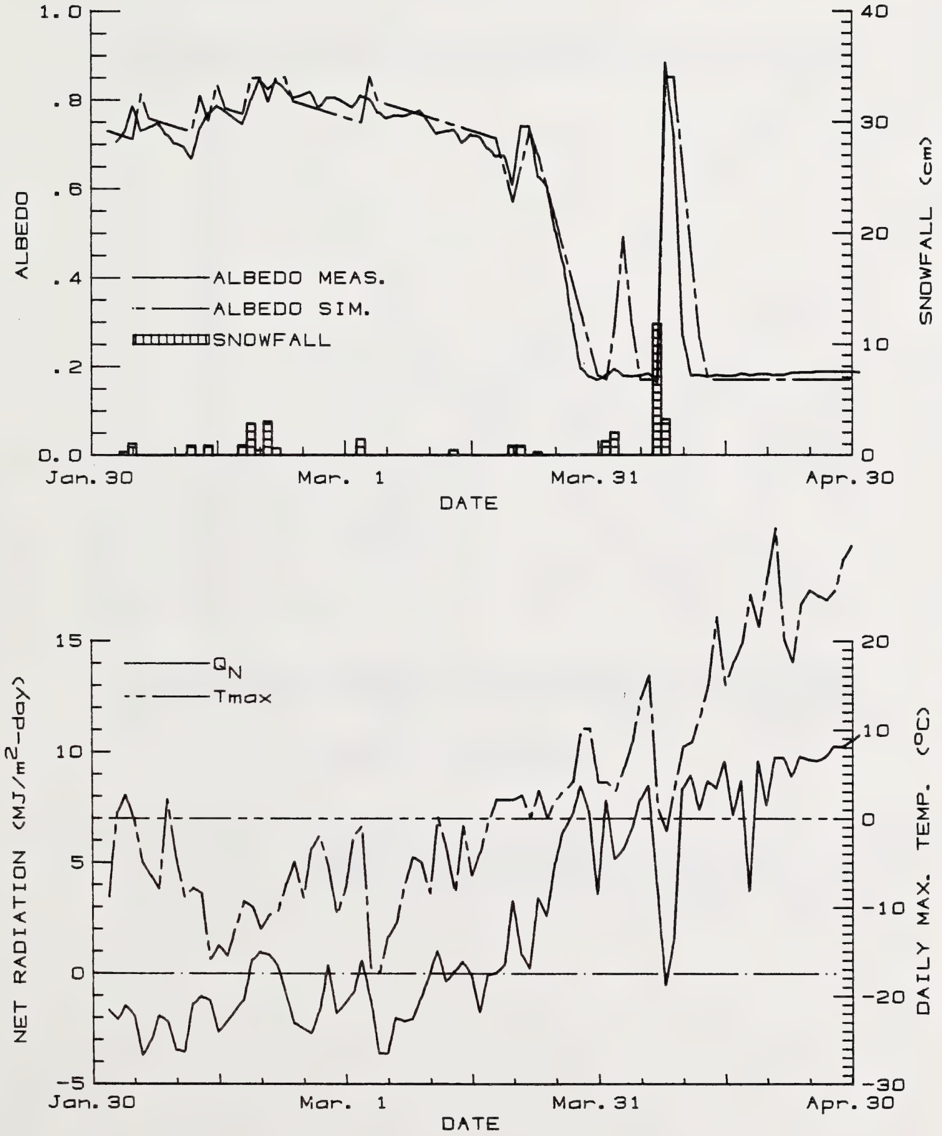

Figure 12. Measured and simulated albedo for a shallow snowcover ($\bar{<}$25 cm) and measured snowfall, net radiation and maximum air temperature plotted with time during Premelt, Melt and Postmelt periods, Bad Lake, Saskatchewan, 1980.

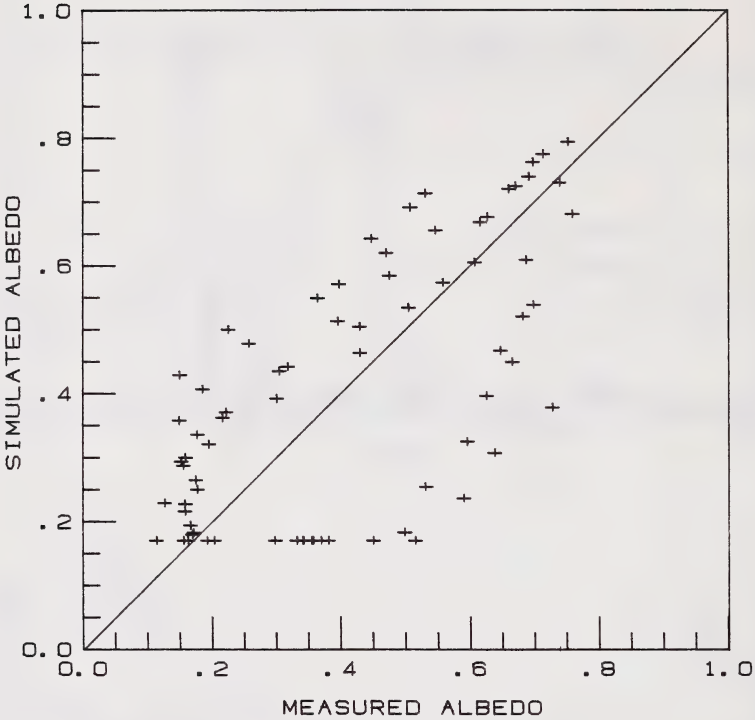

Figure 13. Simulated versus measured albedo for 74 days of melt at Bad Lake, Saskatchewan, 1972-1982.

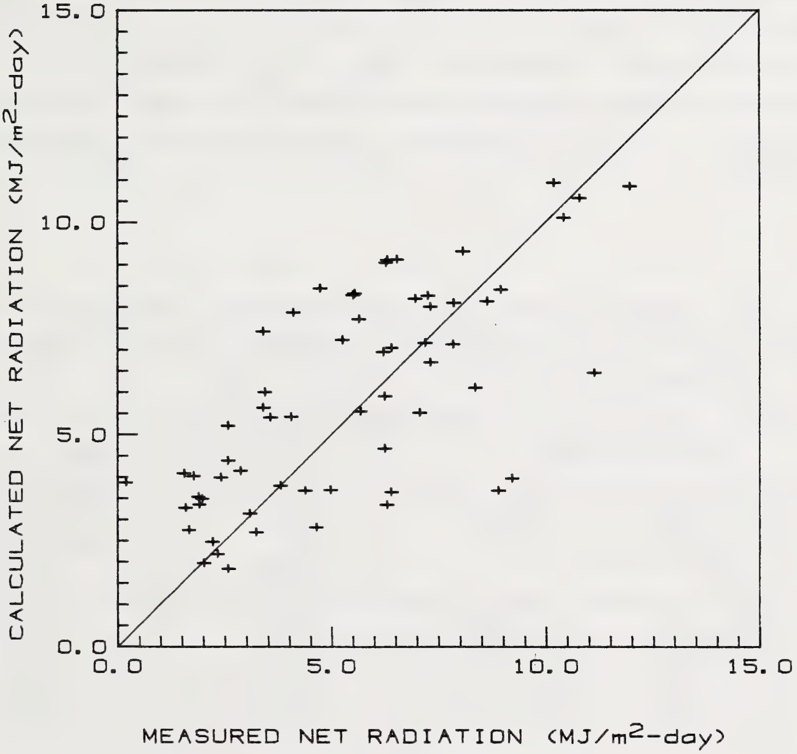

Figure 14. Comparison between calculated and measured net radiation for 67 days of melt, Bad Lake, Saskatchewan, 1972-1982. "Measured" net radiation used to establish "start-of-melt".

snowcover is usually high and fog, haze or ice crystals are commonly present, especially at night and early morning.

The data in Table 3 index the sensitivity of the mean and standard deviation of $(Q_{NC} - Q_{NM})$ to different inputs of short-wave radiation and albedo. From these data it is evident that the differences to the statistical parameters of $(Q_{NC} - Q_{NM})$ caused by the use of empirical estimates of short-wave radiation are small and the model estimates of albedo increased the standard deviation by about 0.5 MJ/m^2-d.

Table 3. Effects of different input parameters on the mean and standard deviation of the difference between calculated (Q_{NC}) and measured (Q_{NM}) daily net radiation during Melt.

Input Parameter		Difference $(Q_{NC}-Q_{NM})$	
Short-wave Radiation MJ/m^2	Albedo	Mean MJ/m^2	Standard Deviation MJ/m^2
Measured	Measured	-0.36	1.44
Measured	Simulated	-0.44	2.07
Calculated	Measured	+0.20	1.59
Calculated	Simulated	+0.49	2.05

The above analysis made use of "measured" values of net radiation during Premelt for establishing the "start-of-melt". An identical analysis was performed on the data in which the Q_N-values during Premelt were calculated by Eq. 11b using estimates of the incident short-wave (Q_s) and net long-wave (Q_{ln}) fluxes obtained by Eqs. 8a and 20a, respectively. A comparison of the calculated and measured net radiation for 60 days of melt is shown in Fig. 15. The mean difference $(Q_{NC} - Q_{NM})$ is 0.76 MJ/m^2 with a standard deviation of the differences of 1.96 MJ/m^2. The positive value of the mean difference suggests a minor trend for the decay in albedo in the model to occur in advance of the monitored depletion.

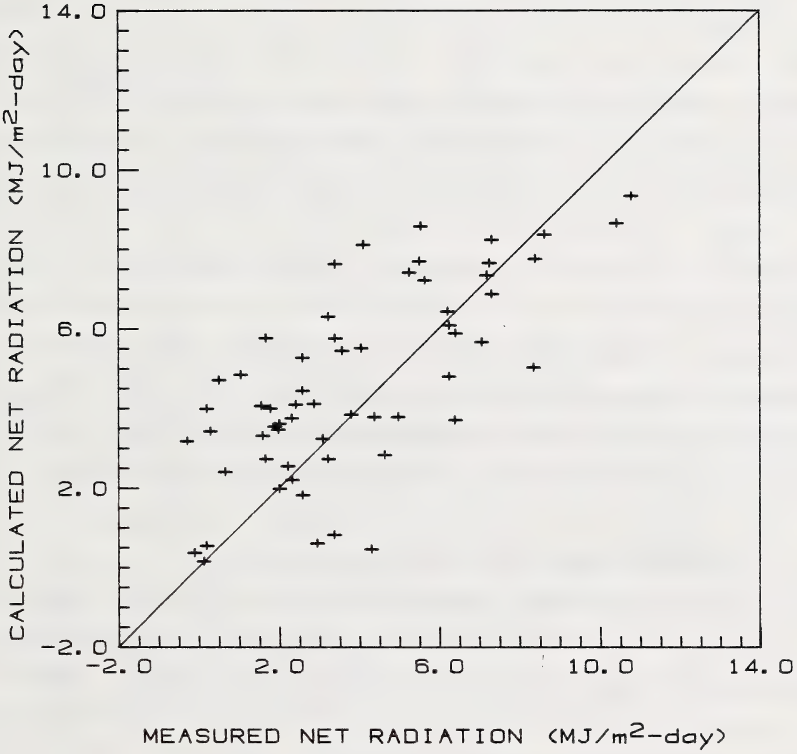

Figure 15. Comparison between calculated and measured net radiation for 67 days of melt, Bad Lake, Saskatchewan, 1972-1982. "Calculated" net radiation used to establish "start-of-melt".

Although a standard deviation of 2.0 MJ/m^2-d, the equivalent amount of energy that would melt about 6 mm of ice at 0° C, is large, it is impossible to reject the estimates of net radiation as being unacceptable for operational purposes. Further work is needed to determine the response of a forecasting system to varying net radiative fluxes on the calculation of snowcover runoff under different melt sequences. However, a sensitivity analysis which would provide this information is beyond the scope of the present investigation. On review of the data in Fig. 15, there is no evidence to suggest that the variance in $(Q_{NC} - Q_{NM})$ increases with the magnitude of the flux. Thus, it is assumed that the relative error to a snowmelt calculation caused by an inaccurate estimate of net radiation would likely decrease as melt progresses. Granger (1977) found maximum melt rates for deep, "complete" Prairie snowcovers on stubble to range from 5 to 7 mm/d and Erickson et al. (1978) reported maximum runoff rates in the range of 18 to 23 mm/d for patchy snowcover conditions on fallow.

3.5 CONVECTIVE ENERGY FLUXES

The convective fluxes of sensible and latent energy are often of secondary importance to net radiation during the early stages of melt of a complete snowcover in the Prairie region. However, as the snowcover becomes discontinuous and energy derived from bare ground is advected to adjacent patches of snow, these fluxes play an increasingly important role in snowcover ablation.

Both the sensible and latent fluxes are governed by the turbulent energy exchange processes occurring in the 2 or 3 m layer of the atmosphere immediately above the snow surface. For a snow-covered surface, techniques are available which may be used to evaluate these components, for example eddy correlation methods, from profiles of wind, temperature and windspeed and others. However, most of these procedures are not practical for operational use because of the number of variables which need to be measured and the sophisticated instrumentation required for these observations. Further, the mechanisms of convective energy transfer under patchy snowcover are not well-understood, nor have practical methods for estimating their magnitudes under these boundary conditions been developed. Because of these limitations and the requirement that the snowmelt model use readily-available meteorological data, the terms were estimated by bulk, semi-empirical expressions.

3.5.1 Sensible Heat

Granger and Male (1978) proposed an expression for estimating the sensible heat transfer (Q_h) from the energy content of an air mass as indexed by the upper air temperature at 85 kPa (T_{85}) of the form:

$$Q_h = 0.283 + 0.279\, T_{85} + 0.013\, T_{85}^2 \quad , \qquad .22$$

in which Q_h is in MJ/m^2-d and T_{85} is in $^{\circ}$C. Equation 22 has the advantage of simplicity, making use of a single atmospheric parameter. Its' principle application is to situations where the major transfer of energy occurs from a large air mass (e.g. chinook), when local advection is negligible (complete snowcover), and a front is not located between the catchment and the point of measurement of T_{85}. Unfortunately, Eq. 22 is usually limited in application by the small number of stations that record T_{85}.

The common bulk aerodynamic expression used to evaluate Q_h has the form:

$$Q_h = D_h\, U_z\, (T_a - T_s) \qquad .23$$

where:

D_h = bulk transfer coefficient for convective heat transfer (kJ/m^3-$^{\circ}$C),

u_z = windspeed at some reference height z-usually taken between 1 and 2 m (m/s), and

T_a, T_s = temperatures of the air and snow surface respectively ($^{\circ}$C).

Daily estimates of Q_h calculated by Eq. 23, using a value for D_h = 0.00106 kJ/m^3-$^{\circ}$C suggested by Hicks and Martin (1972), are compared with the corresponding values obtained from detailed profile measurements (Granger 1977) for two years of snowmelt at Bad Lake, Sask., in Table 4. It is evident from these data that the differences vary widely with the values estimated by Eq. 23 being smaller than the profile estimates. Part of the differences can be attributed to the fact that the profile estimates are based on hourly data whereas Eq. 23 makes use of the daily mean temperature and T_s was assumed to be 0^oC. However, because the differences vary in sign (negative versus positive) no attempt was made to revise Eq. 23 to obtain closer agreement (Granger suggests $D_h = 0.00669$ kJ/m^3-^{o}C for Prairie snowcovers). Further research directed to the development of improved practical formulations for Q_h, especially for patchy snow-cover conditions, is needed.

Table 4. Comparison of daily estimates of sensible heat during snowmelt (MJ/m^2-d) by Eq. 23 with those calculated by detailed profile measurements.

Date	Method	
Mo/Day/Year	Eq. 23	Profile
04/11/75	-0.83	0.19
12	-0.16	1.08
13	-0.71	-0.14
14	-0.13	0.18
15	-0.18	0.16
03/17/76	-1.08	1.83
18	0.50	1.70
19	0.28	0.58
28	0.03	0.67
29	-0.06	1.07
30	0.18	1.59

In view of the findings above it was decided to develop an empirical expression for Q_h based on the data given by Granger (1977). The "best" two and three-variable correlations found were:

$$Q_h = -0.92 + 0.076u_{10} + 0.19TMAX, \text{ and} \qquad .24a$$

$$Q_h = -1.36 + 0.077u_{10} + 0.16\ \mathrm{TMAX} + 0.90n/N \qquad .24b$$

where:

u_{10} = mean daily 10-m windspeed (m/s),

TMAX = daily maximum air temperature, and

n/N = daily sunshine ratio.

Equations 24a and 24b give Q_h in kJ/m^2-d and have correlation coefficients and standard errors of estimate of 0.76 and 0.82; and 0.55 and 0.51, respectively. The expressions are limited to the months of March and April; to days when TMAX is greater than -5°C and to site, snowcover depletion patterns and climatological conditions similar to those experienced during the two years of measurement.

3.5.2 Latent Energy

The discussions above concerning the transfer of sensible heat by convection also apply to the convective transfer of latent energy (Q_e). However, Q_e is usually much smaller than Q_h. Kuz'min (1972) suggests the following equation for daily evaporation from a snowcover:

$$E = (0.18 + 0.098\ u_{10})(e_s - e_2) \qquad .25$$

where:

E = daily evaporation (mm/d),

u_{10} = mean daily 10-m windspeed (m/s),

e_s = mean daily vapor pressure at the snow surface, usually taken equal to 6.11 mb for a melting snowcover, and

e_2 = actual vapor pressure of the air (mb) at 2 m.

Kuz'min states: "The free term (0.18) in Eq. 25 expresses the effect of heat convection. The formula is applicable only to conditions of medium roughness of the snow surface but is suitable for a wider range of wind speeds (from 0 to 12 to 14 m/s) including the lowest speeds (0 to 2 m/s); this is particularly important because the logarithmic and power formulae do not yield satisfactory results for such speeds".

Table 5 compares estimates of E from Eq. 25 with the corresponding values obtained from detailed profile measurements (Granger 1977) for different days of melt during 1975 and 1976 at Bad Lake, Saskatchewan. It is evident that the Kuz'min estimates are larger than those obtained by Granger. Unfortunately, the melt, snowcover, topography and land-use conditions over which the data used in the development of Eq. 25 are not known (Kuz'min states 357 observations of evaporation - presumably with a small evaporimeter - over durations of 2 to 24 h). Thus, it is difficult to assess the reliability of the expression for estimating evaporation in a Prairie environment. Intuitively, it is suspected the values may be high because: (a) the rates would require very large energy inputs - a sublimation loss of 1.7 mm/d (Table 5) would represent a flux of the order of 4.8 $\mathrm{MJ/m^2}$-d; (b) field measurements over complete snowcovers have shown very small humidity gradients during melt and do not support the proposition of large sublimation/evaporation losses; (c) likely under patchy snowcover the average gradient of latent energy is toward the snowcover - that is, energy is added to the snow surface by condensation; and (d) the ratio of the latent heat of sublimation to fusion is approximately 8.5, thus most of the energy would be used for melt, which in turn would infiltrate into the snowcover. On the other hand, most of Granger's data were collected over complete snowcovers and probably do not accurately reflect the flux of latent heat over patchy snowcover. Because of the lack of other data and having confidence in the measurements from Bad Lake, the values of E obtained by Eq. 25 were adjusted by a factor of 0.24 - the average ratio of values calculated by Eq. 25 and the profile method. Equation 25 was therefore modified to:

$$E = 0.24(0.18 + 0.098\, u_{10})(e_s - e_2) \quad , \qquad .26$$

in which E is in mm/d. Table 5 provides a comparison between daily evaporation by Eq. 26 and the profile method. It is emphasized that Eq. 26 will likely provide low estimates of E during the later stages of melt.

Table 5. Comparison of daily estimates of evaporation during snowmelt (mm/d) by Kuz'min's equation (Eq. 25) with those obtained from detailed profile measurements.

Date	Method		
Mo/Day/Year	Kuz'min	Profile	Modified Kuz'min[a]
04/11/75	-1.32	-0.30	-0.32
12	-0.54	0.01	-0.13
13	-1.05	-0.26	-0.25
14	-0.69	-0.14	-0.17
15	-0.69	-0.29	-0.17
03/17/76	-1.68	-0.19	-0.41
18	-0.60	-0.23	-0.15
19	-0.45	-0.08	-0.11
28	-0.45	-0.07	-0.11
29	-0.75	-0.02	-0.18
30	-0.75	0.05	-0.18

[a] Modified Kuz'min = 0.24*Eq.25.

3.6 GROUND HEAT FLUX

The ground heat flux (Q_g) can be taken as a negligible component in the daily energy balance of a snowcover when compared to radiative and convective terms. For practical purposes it can be assumed constant in the range 0 to 260 kJ/m^2•d (Granger 1977).

3.7 HEAT FLUX FROM RAIN

Assuming rain falling on a melting snowcover does not freeze, the energy supplied by rainfall, (Q_p) in kJ/m^2-d can be estimated by the expression:

$$Q_p = 4.2\ T_r P_r \qquad .27$$

where:

T_r = temperature of the rain (^{o}C), usually taken equal to the ambient air temperature, and

P_r = depth of rain (mm).

3.8 CHANGES IN INTERNAL ENERGY

The internal energy content of a snowcover (u) affects the energy available for melt and the release of meltwater. Shallow snowcovers and the upper layers of deep snowpacks often exhibit diurnal cycles in these patterns, e.g. snow melts in late morning and afternoon and refreezes during the night. The night-time energy deficit must be compensated the following day before a snowcover becomes isothermal at 0^oC and releases water. For deep snowpacks, such as those found in mountainous regions, the diurnal changes in internal energy are usually small and relatively insignificant in magnitude compared to other terms of the energy equation. Therefore, they are frequently neglected in melt calculations.

The internal energy of the snowcover consists of components for the ice, liquid and vapor phases and can be evaluated by the expression:

$$u = d(\rho_i C_{pi} + \rho_\ell C_{p\ell} + \rho_v C_{pv}) T_m \qquad .28$$

where:

u = internal energy,

d = depth of snow,

ρ = density,

C_p = specific heat, and

T_m = mean snow temperature,

and i, ℓ, and v refer to ice, liquid and vapor. Usually the contribution of the vapor phase term to u is negligible and may be neglected. Also, during non-melt periods the liquid volume can be assumed zero, so that the evaluation of u involves measurement of d, ρ_i and T_m (a value for C_{pi} can be obtained from Tables or empirical expressions). For days with melt the relative amounts of water and ice in a snowcover may vary widely between day and night. Monitoring the internal energy change would require detailed, systematic measurements of water and ice contents. At the present time, the only field methods for measuring the internal energy content are dillution techniques and these are unsuitable for operational practice.

Because of the lack of information on density, phase composition and temperature needed to calculate du/dt by Eq. 28, an algorithm was used to approximate the term. In its development two major assumptions were made to simplify the internal energy accounting. The first was that a snowcover reaches a minimum state of internal energy (u_{min}) determined by the daily minimum air temperature (TMIN). u_{min} in MJ/m^2-d is calculated by the expression:

$$u_{min} = 2.5d(2.115 + 0.00779\text{TMIN})\text{TMIN}/1000 \qquad .29$$

in which d is the depth of snowcover in cm and TMIN in ^{o}C. Equation 29 assumes a density for the snowcover of 250 kg/m^3. Note: if TMIN = 0, $u_{min} = 0$. This condition is true for the ice phase, but the liquid content (if any at 0^{o}C) will have an internal energy content (u_ℓ) in MJ equal to:

$$u_\ell = \rho_\ell V_\ell h_f/1000, \qquad .30$$

in which ρ_ℓ = density of water in kg/m^3, V_ℓ = volume of water in m^3 and h_f = latent heat of fusion (333.5 kJ/kg). However, in order to simplify the program logic, the maximum value for internal energy was set to zero. The energy associated with liquid water becomes important only when melt stops. If this occurs, the internal energy is held at zero until the liquid water contained by the snowcover is refrozen.

The second assumption was that no melt occurred unless indicated by the albedo routine, i.e. by a rapid decrease in albedo.

The algorithm used to calculate daily changes in internal energy is shown in Figs. 16a and 16b. Q = sum of the major energy fluxes for the day, neglecting du/dt; u_t, u_{t-1} = internal energy content of the snowcover per unit area on day t and day t-1, respectively (u_t is taken as the sum of the internal energy the preceding day, u_{t-1} plus Q to a maximum value of zero and a minimum value (u_{min}) calculated by Eq. 29); d, d_{max} = current snow depth and the maximum snow depth (cm), respectively; LW_{max} = maximum liquid water capacity

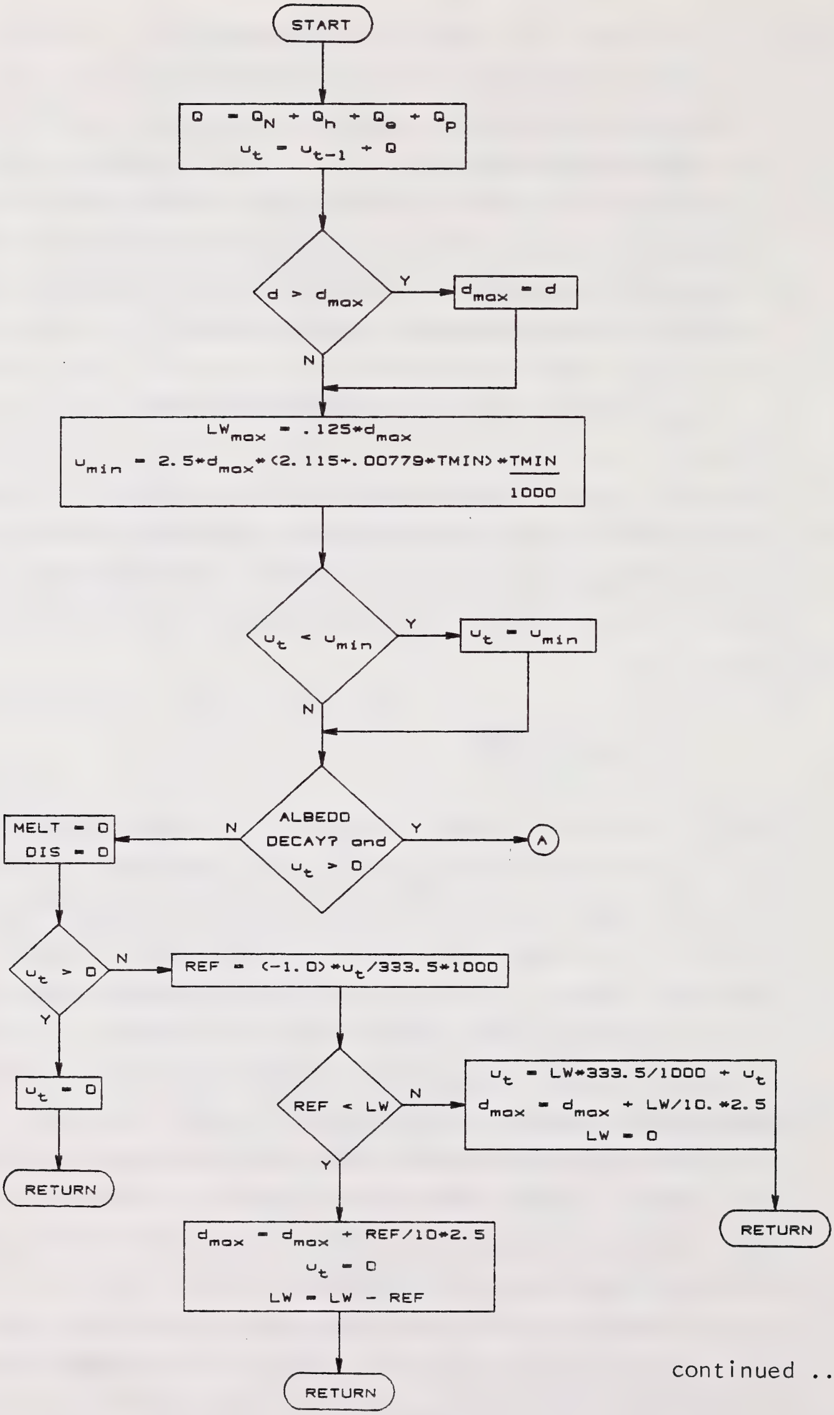
START
Q = Q_N + Q_h + Q_e + Q_p
u_t = u_t-1 + Q
d > d_max
Y
d_max = d
N
LW_max = .125*d_max
u_min = 2.5*d_max*(2.115+.00779*TMIN)*TMIN / 1000
u_t < u_min
Y
u_t = u_min
N
ALBEDO DECAY? and u_t > 0
N
Y
A
MELT = 0
DIS = 0
u_t > 0
N
Y
REF = (-1.0)*u_t/333.5*1000
u_t = 0
RETURN
REF < LW
N
u_t = LW*333.5/1000 + u_t
d_max = d_max + LW/10.*2.5
LW = 0
RETURN
Y
d_max = d_max + REF/10*2.5
u_t = 0
LW = LW - REF
RETURN

continued ...

Figure 16a. Flow Diagram for internal energy accounting.

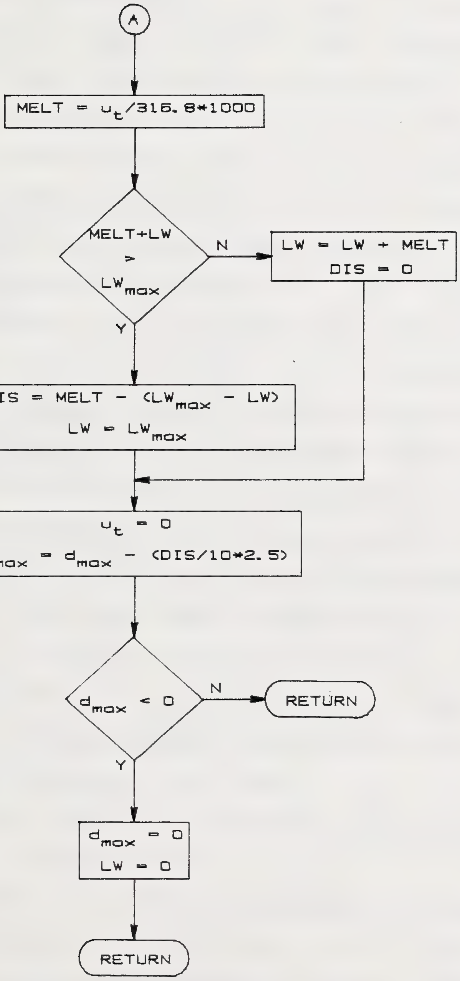

Figure 16b. Flow Diagram for internal energy accounting. Concluded.

of the snowpack; ALBEDO DECAY? = a logical variable which becomes true when the albedo routine indicates that the albedo is decreasing (melt); MELT = daily amount of snow (ice) converted to liquid; DIS = amount of meltwater released by the snowcover; and REF = portion of liquid water storage that can be re-frozen if melt stops.

A brief description of the algorithm follows (refer to Figs. 16a, 16b). Q, the energy available is calculated and used to update the status of the internal energy, u_t (Fig. 16a). The snowcover depth is checked, if it has increased the maximum is updated and this value is used to calculate the maximum liquid water content of the snowpack (LW_{max}). LW_{max} is taken as 5% by weight, which for a snowcover having a density of 250 kg/m^3 is equal to 0.125d (mm) when the snow depth is in cm.

The minimum value of internal energy is calculated by Eq. 29, and the current internal energy u_t is compared to u_{min}, if u_t is less than u_{min}, it is set to u_{min}.

If the albedo routine does not indicate melt, or $u_t < 0$, then MELT and DIS are set to 0. Also, if $u_t < 0$, a portion of the liquid water in the snowpack is re-frozen, the liquid water content is reduced accordingly and the snowcover depth (d_{max}) increased by the amount re-frozen. Conversely, if $u_t > 0$, u_t is set to zero and control is returned to the main program (excess energy is dumped).

If melt occurs and $u_t > 0$, (see Fig. 16b) then MELT in mm/d is calculated by the expression:

$$MELT = u_t/316.8*1000, \qquad .31$$

which is the same as Eq. 2 with M = MELT, $Q_m = u_t$, $\rho = 1000$ kg/m^3, h_f = 333.5 kJ/kg and B = 0.97. If the amount of melt plus the existing liquid water content exceeds the maximum liquid water content, discharge (release of meltwater) begins. Then u_t is set to zero, and the snowpack depth is decreased by the amount of melt. When the snow depth has been decreased to zero, the liquid water content is added to the amount of meltwater released in that day.

4. MODEL PERFORMANCE

4.1 COMPARISON BETWEEN "START" AND "FINISH" OF SNOWCOVER RUNOFF AND DECREASE IN SNOW DEPTH

Figures 17 and 18 show "measured"; snow depth and snow-fall and "simulated"; albedo and accumulated snowcover runoff (meltwater release) plotted with time from Feb. 1st to Apr. 30th for 1974 and 1982 at Bad Lake. The maximum snow water equivalent in 1974 was 143 mm, whereas in 1982 the maximum was 53 mm, near the normal. Because of the abrupt, well-defined change in the temperature and radiation regimes from 'winter' to 'spring' in both years the model produced good simulations of albedo. In 1974, simulated runoff began on April 3, 5 days after the snowcover measurements showed a decrease in mean snow depth. A light snowfall on April 6 halted melt until April 10, then the snow depth and albedo began to decrease rapidly (indicative of "active" melt). The end of runoff and disappearance of the snowcover occurred on the same day.

In 1982, simulated runoff and the rapid decrease in snow depth commenced on April 10, with complete ablation of the snowcover on April 14. As shown in Fig. 18, snowcover runoff was complete before the albedo decreased to its' value for bare ground. This suggests a need for a feedback mechanism which would allow snow depth to control the albedo routine or vice versa.

Figure 19 shows "measured" snow depth and snowfall and "simulated" albedo and meltwater release plotted with time for 1973 at the Regina airport. The model produced runoff beginning one day after the snowcover had disappeared. The root cause of the delay is unknown, however a contributing factor may have been that the increases in simulated albedo by the light snowfall events in mid to late February were overestimated. These storms were accompanied by periods with relatively-high wind speeds (20 to 50 km/h) and it is unlikely there were significant accumulations of snow in exposed areas. This is substantiated by the snow course measurements which showed no increase in the mean depth as a result of the storms. If the effects of the snow falls on albedo were assumed negligible, this would cause a higher net radiative flux and simulated runoff to occur earlier.

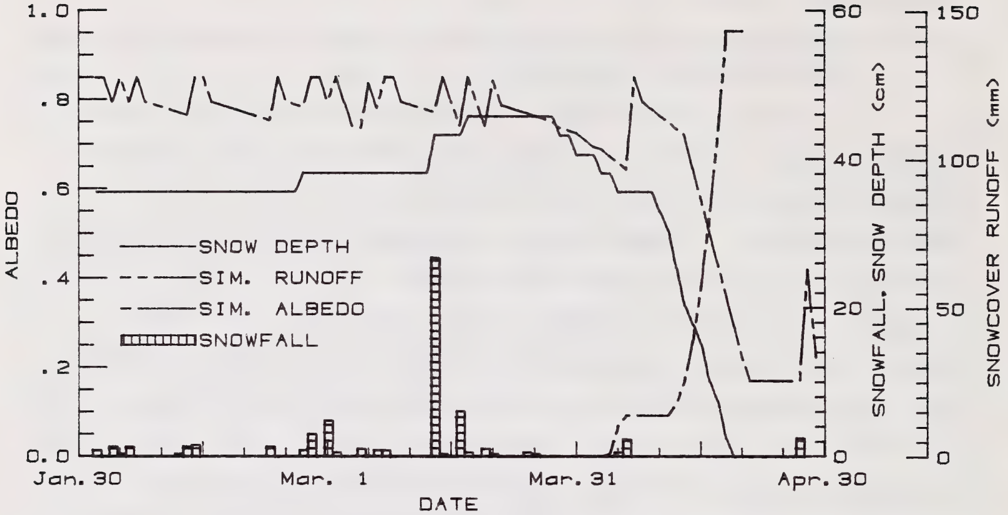

Figure 17. Measured: albedo, snowdepth and snowfall and simulated: albedo and accumulated snowcover runoff for the Bad Lake climatological station plotted with time, Feb. 1 to Apr. 30, 1974.

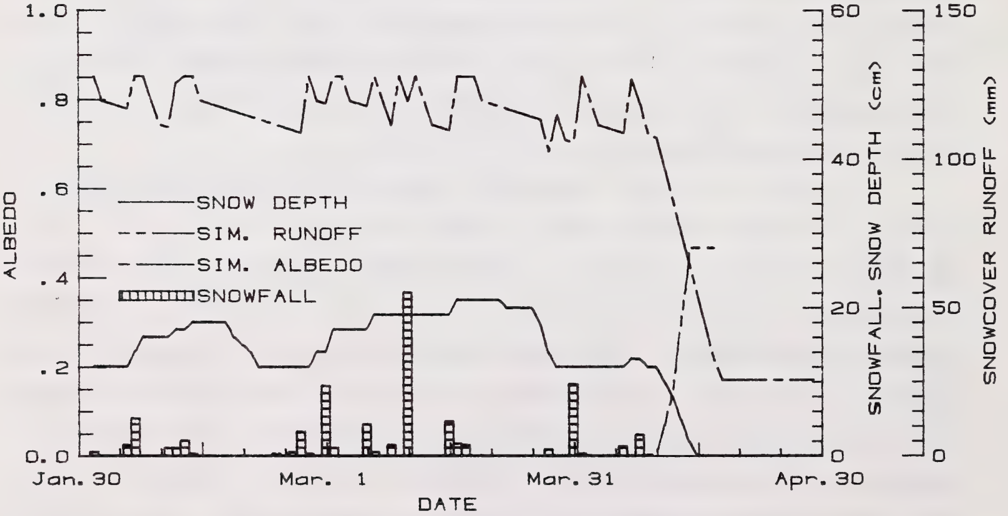

Figure 18. Measured: albedo, snowdepth and snowfall and simulated: albedo and accumulated snowcover runoff for the Bad Lake climatological station plotted with time, Feb. 1 to Apr. 30, 1982.

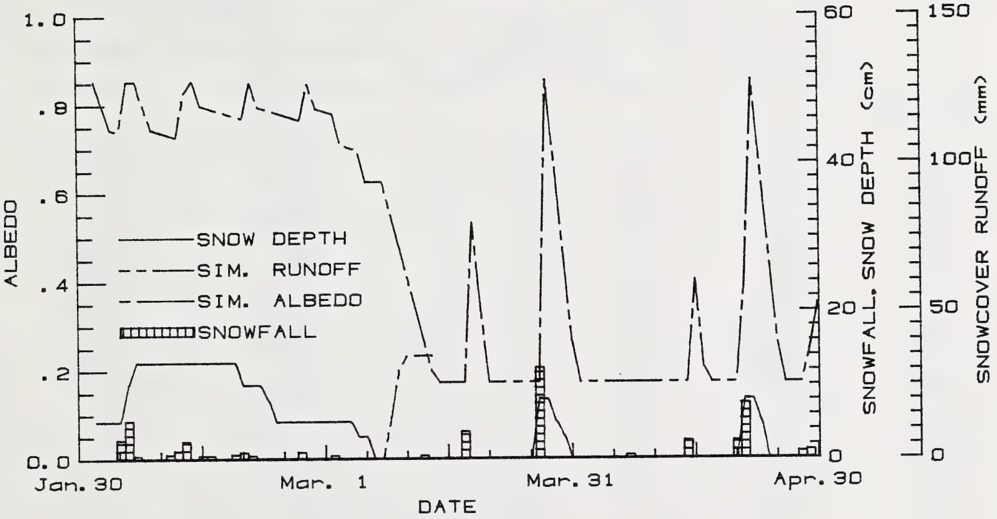

Figure 19. Measured: albedo, snowdepth and snowfall and simulated: albedo and accumulated snowcover runoff for the Regina airport plotted with time, Feb. 1 to Apr. 30, 1973.

Table 6 lists the Julian day in different years, "simulated" runoff, and the decrease in snow depth started and finished at the Bad Lake and Regina stations. The mean difference between the start of runoff and decrease in snow depth was 2.2 days. The trend for runoff to lag a decrease in depth is expected as a snowcover will store water, densify, and consolidate prior to releasing meltwater. These findings suggest the need for a routing routine that will account for the effects of the snowcover on the vertical movement of melt quantities generated at its' surface.

The mean of the annual differences between the end of runoff and complete ablation of the seasonal snowcover was -0.6 days, despite the wide range in annual values from -9 to +10 days.

Table 6. Julian day of "Start" and "End" of simulated snowcover runoff and decrease in measured snow depth at Bad Lake and Regina.

	Start			End		
Year	Sim.Runoff	Diff	Decrease in Snow Depth	Sim.Runoff	Diff	Ablation
Bad Lake						
1972	75	5	70	83	-9	92
1974	93	5	88	108	0	108
1976	78	0	78	89	-8	97
1977	64	0	64	66	0	66
1978	82	1	81	88	-3	91
1979	66	2	64	76	-2	78
1980	79	0	79	85	-3	88
1981	49	2	47	53	0	53
1982	100	0	100	104	0	104
1984	80	0	80	83	-2	85
Regina						
1972	75	3	72	91	-1	92
1973	63	0	63	69	3	66
1974	101	6	95	110	-1	111
1975a	76	3	73	79	2	77
1975b	101	1	100	109	2	107
1976	86	-1	87	92	-3	95
1977	50	2	48	64	-2	66
1978	69	2	67	79	-2	81
1979a	82	7	75	84	1	83
1979b	106	1	105	111	0	111
1980	89	6	83	96	4	92
Mean		2.2			-0.6	
Std.Dev.		2.3			3.9	

[a,b] Interrupted periods of melt.

4.2 COMPARISON BETWEEN START OF SIMULATED AND OBSERVED RUNOFF

Table 7 lists the accumulated snowfall water equivalent up to the time of melt; the Julian day of the "Start" of simulated runoff-based on climatological data from the Regina airport; and the Julian day of the "Start" of observed streamflow from snowmelt on the Davin and Wascana Creek watersheds. The Davin watershed is a small sub-basin (area = ~ 10 km^2) of Wascana Creek (effective area = ~ 350 km^2).

Table 7. Julian day simulated snowcover runoff at Regina and observed streamflow on Davin and Wascana Creek watersheds started.

Year	Snowfall[a] Water Equiv. mm	Start of Runoff		
		Simulated	Davin	Wascana
1972	103	76	76	81
1973	44	67	64	72
1974	165	103	98	104
1975b	56	76	75	77
1975c	96	101	101	105
1976	128	86	81	94
1977	37	52	64	74
1978	61	69	79	85
1979b	99	82	81	
1979c	139	101	101	110
1980	85	90	81	89
1981	39	51	68	69

[a] Long-term average snowfall water equivalent for Regina is 116 mm.

[b,c] Interrupted periods of melt.

Comparing the "Start" of simulated runoff with the "Start" of observed flow from the two watersheds the range in annual differences vary from -17 to +5 days for Davin and -22 to +1 days for Wascana Creek. The differences between the time of occurrence of streamflow from Davin and Wascana Creek range from -1 to -13 days.

That the "Start" of streamflow on Davin frequently occurs before simulated snowcover runoff at Regina can be attributed in part to the fact that the snow depth and water equivalent inputs to the model were probably larger than conditions on the watershed. In years with near or above normal snowfall the average ratio on March 1st between the snowfall water equivalent at Regina and the snowcover water equivalent on Davin was 0.68. A proportional decrease in snow water equivalent in the simulations would advance the "start" of snowcover runoff by an average of approximately 1d. In general, except for years with low snowfall the agreement between the start of simulated flow and observed flow on Davin is reasonable.

It can be observed from the data in Table 7 that the largest differences between simulated runoff and observed flow from both watersheds occur in years with below normal snowfall, specifically 1977, 1978 and 1981. In these years, "observed" flow lagged "simulated" snowcover runoff by 8, 10 and 16 days on Davin and by 22, 16 and 18 days on Wascana Creek, respectively. Excluding these years, streamflow on Davin occurred, on average, about 2.5 days before simulated runoff; on Wascana Creek about 3.5 days after. Note the mean difference in the "Start" of flow between Davin and Wascana Creek was 6.5 days.

The fact that streamflow frequently occurs later than surface runoff from adjacent lands in years of low snowfall may be attributed to numerous factors. On the Prairies snowfall is redistributed by wind and in low snow years the major accumulations are found in local depressions, drainageways, and to the lee side of vegetative and topographic barriers. Snow-filled gullies are capable of storing large quantities of water and retarding outflow. Gray et al. (1985) cite the results from an in-channel snow survey conducted near Regina in 1966 which showed 12322 m^3 of water /1000 m of channel when the snowcover had virtually disappeared from adjacent fields and before significant streamflow. The mechanics of water movement in snow-filled channels is not understood. Field observations have indicated however, that significant streamflow does not occur until a channel through the accumulations develops. Essentially, the development of channels causes the dynamics of the flow regime to change from movement through a porous medium to open channel flow. Lateral inflow of surface runoff to drainageways hastens the formation of channels by supplying energy for melt, and by eroding and transporting snow crystals. Melt and meltwater release from snow-filled channels may also be delayed due to shading by the channels.

Further research is needed into the effects of snow on the storage and movement of water in channels so that an algorithm of the process can be developed. At present, because of the lack of understanding of the phenomenon it is probably best in a practical modelling scheme to account for these effects by lagging snowcover runoff a fixed time.

Unfortunately, procedures are not available for calculating the lag time directly, hence the parameter must be determined from trial and error calibration tests on an individual basin.

4.3 STREAMFLOW SIMULATIONS

4.3.1 General

The Energy Budget Snowmelt Model (EBSM) was incorporated into the U.S. Corps of Engineers Streamflow Synthesis and Reservoir Regulation Model (SSARR) and used to synthesize streamflow from snowmelt on the Creighton Tributary and Wascana Creek watersheds in Saskatchewan. The version of SSARR used in the simulations included the algorithm developed by the Division of Hydrology (Gray and Landine 1985, 1986), the "Prairies Option", describing infiltration to frozen prairie soils.

Creighton Tributary is a small (11.4 km^2) sub basin of the Bad Lake Watershed, which is located near Bickleigh, Sask., approximately 165 km southwest of Saskatoon in the semi-arid region of the Province. Wascana Creek at Sedley is located approximately 50 km southeast of Regina and has a "gross" drainage area of about 350 km^2. Both watersheds fall in the Dark Brown soil zone and approximately 85% of the area of each is under cultivation of cereal grains by dryland farming. The Creighton Tributary is a well-defined basin with gently and moderately rolling topography and falls in a transition zone dividing glacial and lacustrine soils. Conversely, the primary soil texture of Wascana Creek is a heavy lacustrine clay on flat to gently rolling topography. Relief of the basin is very poor and the percentage of the gross drainage area that contributes to streamflow may vary widely from year to year.

Climatological data used in the simulations for the Creighton Tributary were obtained from the Bad Lake Climatological Station which is located immediately adjacent (~3 km) to the watershed. For Wascana Creek, weather observations recorded at the Regina Airport (~50 km northwest of the watershed) were used.

All model parameters used in the simulations, for example the routing coefficients, were based on previous studies with the model on the catchments (see Gray and Landine 1985).

4.3.2 Implementation of EBSM in SSARR

4.3.2.1 Input data. In the simulations, the output from the EBSM was used as input to SSARR. To accomplish this, because SSARR only accepts melt rates expressed in mm/d-°C (for use in the degree-day method) and the output from EBSM is in mm/d, changes had to be made to the input and snowmelt subroutines of the model.

Constraints were imposed on modifications to the Input Section so as to avoid extensive and complicated changes in the program. The alterations to the subroutine simply involved additions to the "Prairies Option" (input to Column 17 of the "CB01" card). The options added were:

4 - original SSARR with EBSM,
5 - Limited infiltration with EBSM,
6 - Unlimited infiltration with EBSM, and
7 - Restricted infiltration with EBSM.

Options 4 through 7 input melt quantities on "4D" cards using a type code 9, which in the original model are reserved for melt rates. Thus, no changes were made to the input subroutine coding, only the operating instructions were altered.

4.3.2.2 Basin processing routines. Subroutine BASELINE was modified to check the "Prairies Option" for values of 4 or greater and to set a flag (Melt - OP) for use by subroutine BASEC. If Melt - OP is equal to 1 then the data inputted as type code 9 are interpreted as melt quantities. All calculations of melt used in the original SSARR are ignored, with the exception that melt is assumed to occur over the entire watershed.

4.3.3 Creighton Tributary

Simulations were carried out on the Creighton watershed for 1974 and 1975. As discussed in a previous report (Gray and Landine 1985) these two years provided contrasting snowcover and premelt soil moisture conditions on the watershed. The winter of 1973/74 was a year of near record snowfall which produced a snowcover having an average depth of approximately 565 mm and a water content of 143 mm. The winter was preceded by a warm, dry fall that resulted in the soil moisture status of the 0 to 300 mm layer being very low (average - 15% by volume). In 1974/75 the average depth and water equivalent of the snowcover on the watershed were 299 and 71 mm, respectively, and the average fall soil moisture was 27.4% by volume.

Figures 20 and 21 show the observed and simulated hydrographs from snowmelt. In the figures, SSARR designates the hydrograph generated by the unrevised model (the temperature index approach is used to calculate melt rates) and EBSM - the hydrograph produced by the system with the EBSM routine. Note, because the watershed is relatively small and well-defined, the melt sequences uninterrupted and the depth of snowcover was "normal" or above in each year, the simulated hydrographs were not lagged. Also no attempt was made to shift the simulated hydrographs to a position of "best-fit" with the observed.

In 1974, both EBSM and SSARR reproduced the observed hydrograph reasonably well (Fig. 20). The respective values for "efficiency" R^2 (Nash and Sutcliffe 1970) were 0.65 and 0.58. That the positive value of R^2 given by the EBSM is closer to unity suggests a slightly better simulation with this model.

In 1975 the EBSM gave the closer simulation of observed discharge with an R^2-value of 0.90 compared to -1.28 with SSARR. The reason for the better performance was that the EBSM predicted the start of streamflow within a day of measured flow whereas runoff from SSARR started 5 days late. In the EBSM surface melt began Apr. 13 due to positive fluxes of net radiation and daily maximum air temperature $>0^\circ C$. Melt in SSARR did not begin until Apr. 16 when the daily mean temperature exceeded the threshold of $1^\circ C$.

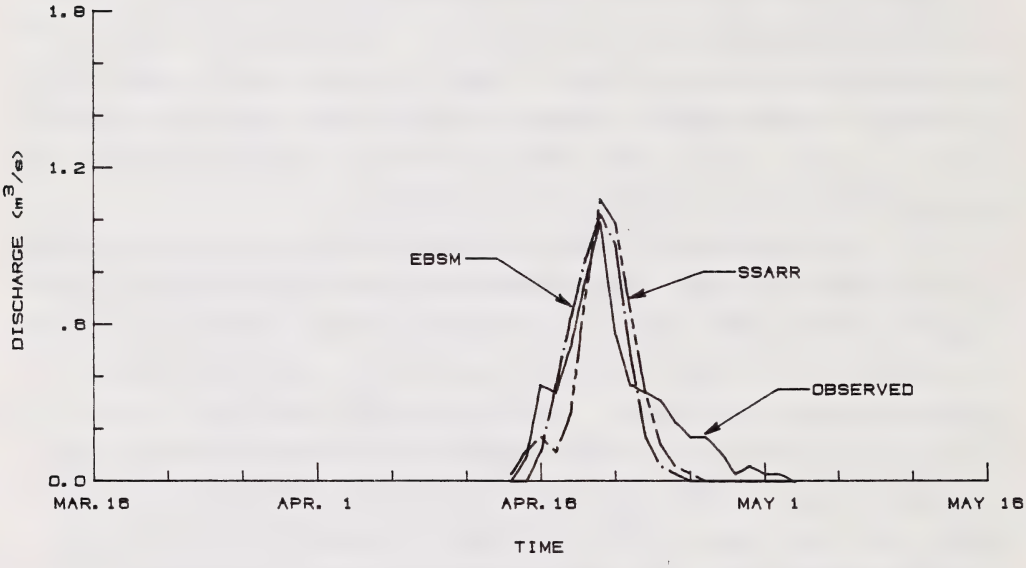

Figure 20. Observed and simulated hydrographs from snowmelt; Creighton Tributary, 1974. SSARR - hydrograph generated by the original system (degree-day method used to calculate melt rates), EBSM - hydrograph generated by SSARR with the energy budget snowmelt routine.

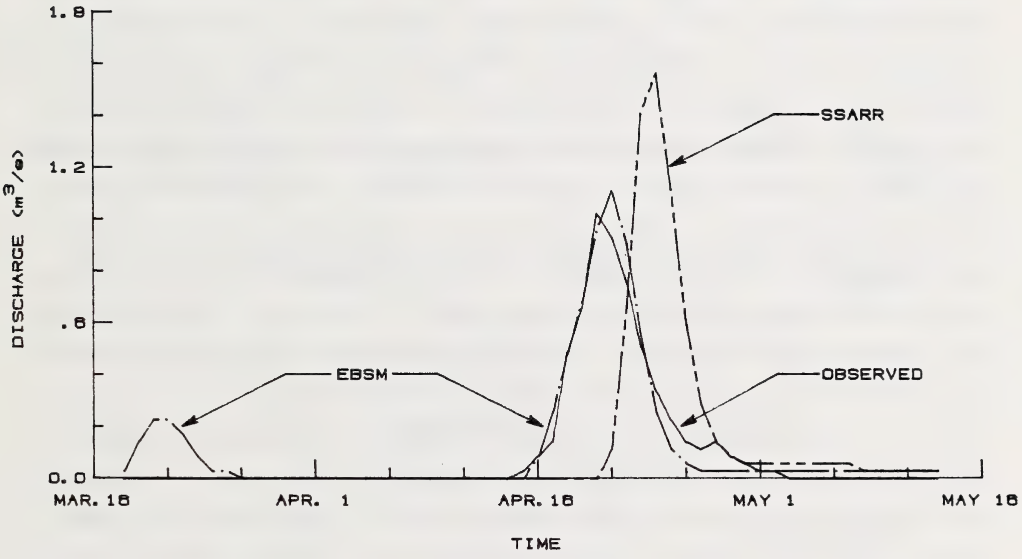

Figure 21. Observed and simulated hydrographs from snowmelt; Creighton Tributary, 1975. SSARR - hydrograph generated by the original system (degree-day method used to calculate melt rates), EBSM - hydrograph generated by SSARR with the energy budget snowmelt routine.

The data in Fig. 21 point out a major weakness and limitation in the current version of the EBSM; namely its' inability to account for the storage and refreezing of quantities of meltwater in excess of the liquid water holding capacity of the snowcover that occur from intermittent periods of melt. Excesses may accrue from the accumulation of meltwater within a snowcover above a layer of restricted permeability, such as an ice lense; meltwater drainage, water ponded on the soil surface, or in movement as overland flow. Allowing water to be released from the snowcover leads to an underestimate in the amount of snow water available for runoff at a later date. Figure 21 shows the EBSM simulated runoff between Mar. 17 and Mar. 30; however, no streamflow was observed (visual observation; gauging station was not in operation). A review of the climatological records showed positive net radiative fluxes between Mar. 17 and Mar. 23 with maximum air temperatures below $0^{o}C$. These conditions are conducive to surface melt and refreezing of the meltwater in the snowcover.

The effect of early season melts on the agreement between simulated and observed hydrographs produced by the seasonal snowcover is illustrated in the data for Wascana Creek in 1979 (see Fig. 22b). Between Mar. 22 and Apr. 1, 1979 the daily net radiation fluxes were positive (Fig. 22a) and resulted in a net energy flux that produced 35 mm of snowcover runoff. The effect of the loss of snow water is demonstrated by the poor agreement between simulated (EBSM) and observed hydrographs starting Apr. 20 (Fig. 22b). Similar results were obtained in other years. Figure 22b also shows the improvement in the simulation when the radiation melt quantities are retained as snow water (hydrograph labelled as MOD EBSM in the figure). Note, it is anticipated that a better fit between simulated and observed hydrographs could have been achieved by modifying the routing coefficients of SSARR.

It follows from the above that the EBSM in its present form will not provide reliable simulations of streamflow in years frequented by periodic, short-duration melt events and work directed toward the development of an algorithm describing the movement and storage of meltwater through the snowcover and refreezing of these quantities is needed.

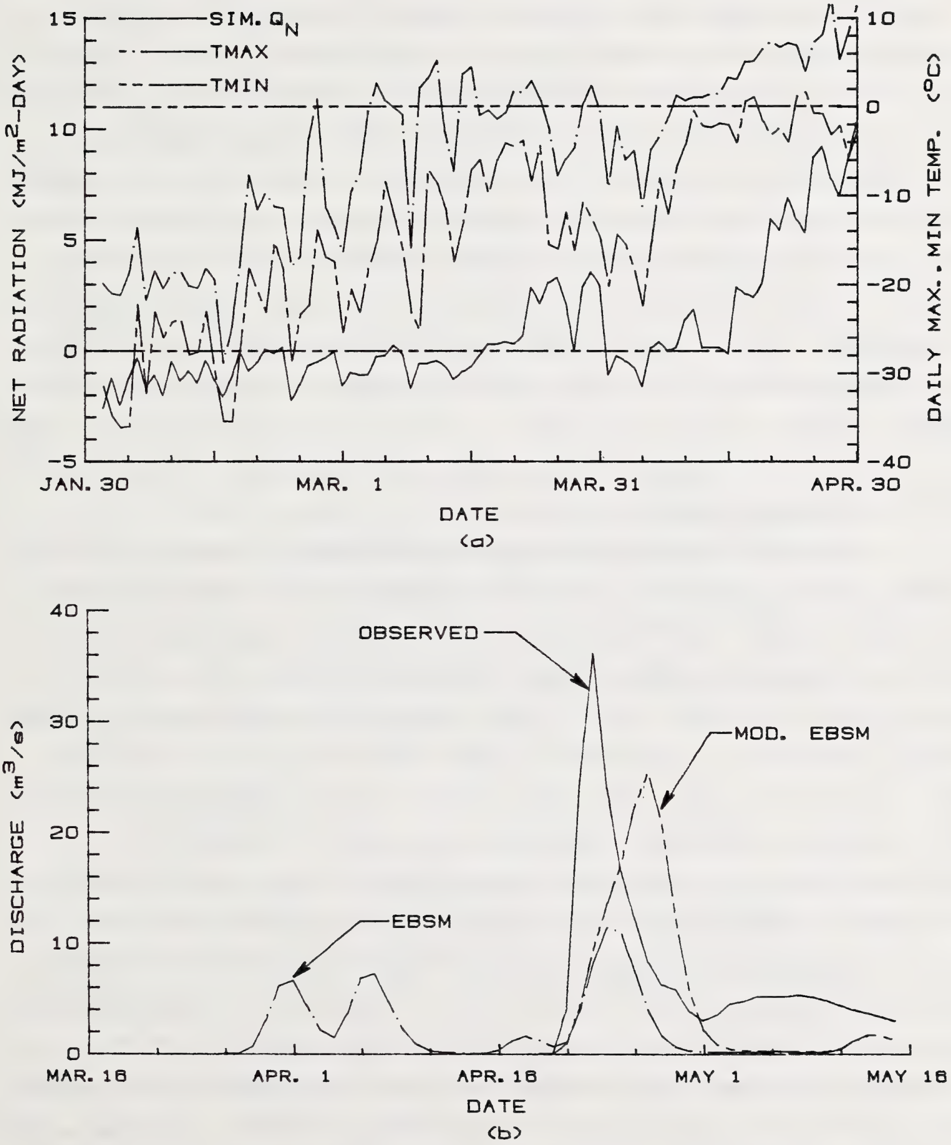

Figure 22. Climatological data for Regina Airport and runoff hydrographs for Wascana Creek, 1982. (a) Simulated net radiation (SIM.Q_N) and maximum (TMAX) and minimum (TMIN) air temperature plotted with time: (b) Observed and simulated hydrographs from snowmelt; EBSM - hydrograph simulated by SSARR with the energy budget snowmelt model, MOD.EBSM - hydrograph simulated by SSARR with the EBSM when it is assumed that snowcover runoff quantities from early melt periods are retained by the snowcover.

In a like manner, the data in Figs. 21 and 22 point out that the degree-day approach is unable to account for radiation melt occurring over short periods in late winter and early spring. No discharge is simulated by SSARR from either Creighton or Wascana Creek prior to the start of complete ablation of the seasonal snowcover. The difference in response of the two models to radiation melt events is simply due to the fact that the EBSM considers all factors affecting the energy exchange whereas SSARR responds only to air temperature. As shown in Fig. 22a, only 3 days in the period between Mar. 22 and Apr. 1, when the net radiative fluxes were positive and there was energy available for melt, was the maximum air temperature above 0°C.

4.3.4 Wascana Creek

Streamflow simulations were undertaken on Wascana Creek at Sedley, Sask., for 1972, '74, '76, '79 and '80. The material below discusses the pertinent results of this analysis. In these discussions no attempt is made to draw final conclusions on the relative performance of the two models (EBSM and SSARR) in synthesizing observed flow. The manner in which the routing coefficients were determined and the different ways the effects of storage on runoff are handled by the models negate this evaluation. As stated in Section 4.2, Wascana Creek is a poorly-drained watershed in which storage has a pronounced effect on the shape of the discharge hydrograph. The routing coefficients used in the simulations were established from calibration tests performed on the basin with the unrevised SSARR and represent those values which provide good representation of the observed hydrograph when the melt rates are calculated by the degree-day method. The coefficients for the EBSM will differ. Further, the simulated hydrographs from the EBSM were lagged three days in attempt to account, in part, for the effects of storage on the movement of melt quantities (see discussion in Section 4.2).

Figures 23 and 24 show simulated and observed flows for two years; 1972 - a low flow year and 1974 - a high flow year. The respective values of efficiency (R^2) with the EBSM were -0.01 and -0.08

and with SSARR, -0.05 and 0.37. These R^2-values suggest comparable, but poor agreement between simulated and observed hydrographs by the two models in 1972. Unfortunately, insufficient data are available to explain the lack of agreement, however it is presumed the runoff pattern may have been strongly affected by the variable distribution of snowcover (because of the low snowfall), by the rainfall showers that occurred on Mar. 19 and 20, and Apr. 8 and by the effects of in-channel storage. Also, the fact that the shape of the observed hydrograph differs significantly from the "normal" runoff pattern on the basin - which shows only a single peak - suggests there could have been a gauging problem. However, it is important to note that the EBSM predicted the day of "start" of streamflow exactly whereas SSARR produced runoff three days before measured discharge.

In 1974, the major differences between the simulated and observed flows were: SSARR showed discharge starting 5 days before measured flow and a sharp decrease in discharge rate between Apr. 15 and 17; and EBSM gave a hydrograph with a much flatter rising limb. It is expected that the difference in slope could be decreased by changing the routing coefficients.

4.3.5 Discussion

The results of the simulations with the EBSM on snowcover ablation and streamflow demonstrate that the model is workable and when interfaced with a streamflow forecasting system will provide information on discharge rates of at least equivalent accuracy to that obtained by a temperature index approach. In fact there is evidence, although not conclusive, to suggest that the estimates of the time-of-start and daily snowcover runoff quantities by the EBSM may be better.

The major advantage of the EBSM over a temperature index model is it is based on a physical framework (the energy equation). Hence, changes can be introduced to the system as improved methods and procedures for evaluating the different terms are developed. Also, the model permits greater flexibility and transposibility in application. For example; the effects of changes in slope, latitude,

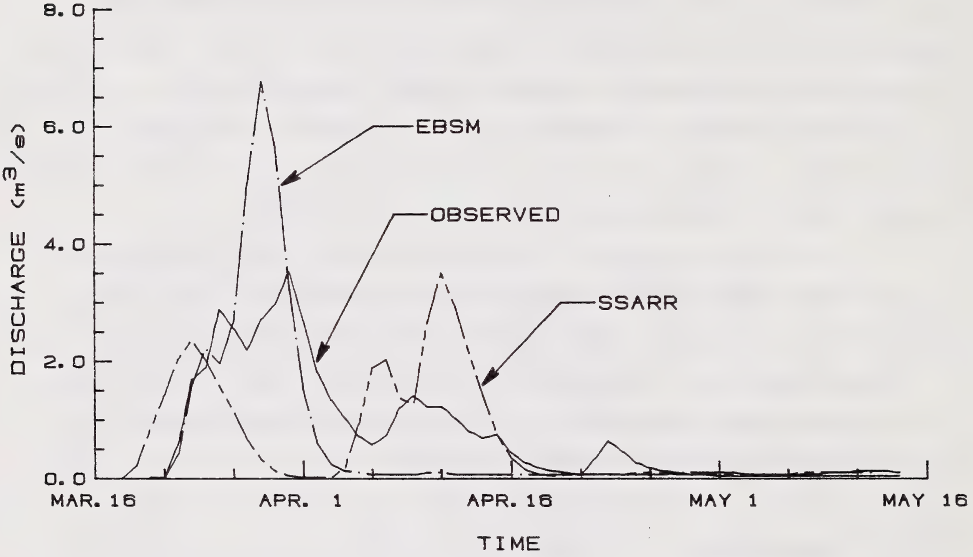

Figure 23. Simulated and observed hydrographs from snowmelt on Wascana Creek at Sedley for a low flow year, 1972. EBSM and SSARR - hydrographs simulated with snowmelt calculated by the energy budget snowmelt model and the degree-day method, respectively.

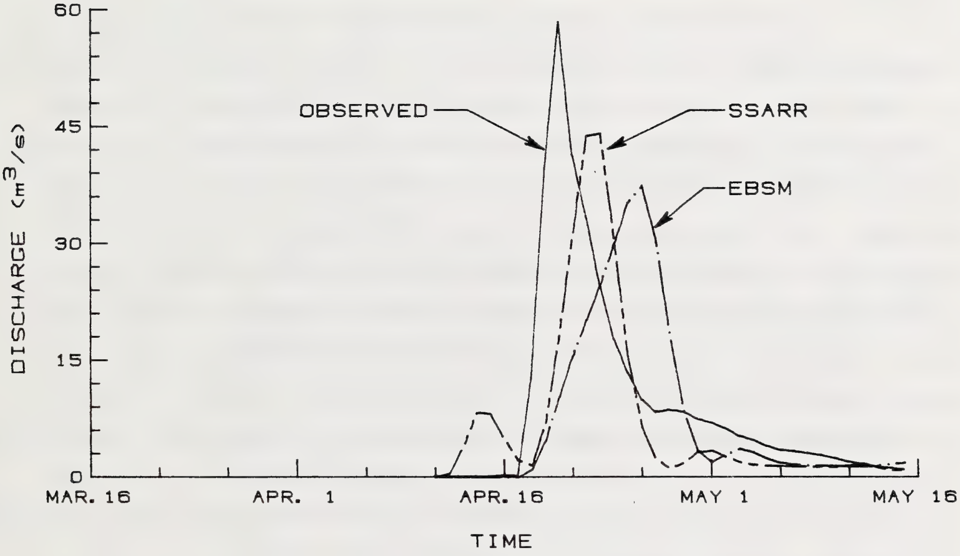

Figure 24. Simulated and observed hydrographs from snowmelt on Wascana Creek at Sedley for a high flow year, 1974. EBSM and SSARR - hydrographs simulated with snowmelt calculated by the energy budget snowmelt model and the degree-day method, respectively.

atmospheric variables, albedo and other factors affecting snowmelt can be calculated directly, not compensated by an adjustment to or recalibration of the melt factor. A disadvantage is it requires a larger data base, namely: measurements of sunshine hours, relative humidity, wind speed, maximum and minimum air temperature. However, these observations are routine at many network stations and, if the variables need to be evaluated, they can be measured with relatively-simple equipment.

It is felt that the results are sufficiently encouraging to support additional work directed to the refinement and verification of the EBSM. Specifically, the transposibility of the empirical coefficients and relationships that have been presented need to be established. The fact that the EBSM, which is based on data acquired at Bad Lake, provided reasonable estimates of snowcover depletion at Regina, and runoff from Davin and Wascana Creek watersheds, suggest that the relationships used to evaluate the components of the atmospheric radiation field may be successfully applied over relatively-large spatial regions of the Prairies. Further studies are needed for the development and refinement of procedures for evaluating the sensible energy flux, particularly over patchy snowcover conditions and the development of an algorithm that will account for storage and refreezing on the release and movement of meltwater quantities.

Ideally, an experimental study should be undertaken on a watershed to acquire data which would allow verification of the EBSM and a comparison of its' performance in snythesizing streamflow from snowmelt with other methods. In this regard it is believed that an extensive measurement program is not required; rather, the observations should be planned and selected to satisfy the needs of the model and the study objectives.

5. SUMMARY

An Energy Budget Snowmelt Model (EBSM) that can be incorporated into operational systems and used to forecast streamflow from snowmelt in open grassland regions is developed and evaluated.

Methods and procedures for estimating the magnitudes of different terms of the energy equation in the model are described.

1. Daily Atmospheric Net Radiation Flux from:
   (a) Empirical relationships derived from 14 years of daily climatological observations for the months of Feb. to Apr. inclusive at Bad Lake, Saskatchewan. The expressions use the extraterrestrial flux and atmospheric transmissivity and standard observations of air temperature, relative humidity, wind speed and sunshine hours.
   (b) An albedo-depletion model describing the decrease in albedo with time of shallow snowcovers not subjected to frequent melt events. Depletion is approximated by three line segments of different slope which encompass the periods of Premelt, Melt and Postmelt. During Premelt, albedo decreases slowly with time at a rate of about 0.006/d; during Melt at 0.071/d and following the disappearance of the seasonal snowcover the albedo is constant at 0.17, except when increased by late-occurring snows. The start of Melt is established by an algorithm which considers daily inputs of snow depth, snowfall, net radiation, a threshold air temperature and maximum and minimum air temperatures.

   Comparisons between daily net radiation, calculated by the empirical expressions and the albedo model, with measured fluxes for 62 days of Melt show a mean difference of 0.49 MJ/m^2-d and a standard deviation of 2.05 MJ/m^2-d. Approximately 0.5 MJ/m^2-d of the standard deviation can be attributed to the simulated albedo.

2. Sensible and latent energy fluxes from empirical relationships that employ the mean daily 10-m windspeed and relative humidity and the maximum air temperature. The need for research directed towards the development of improved methods of estimating the convective terms over patchy snowcover is emphasized.
3. Ground heat flux is considered negligible.
4. The advective energy flux by rain from the depth of rain, assuming rain is at the ambient air temperature.
5. Internal energy from snowcover depth and minimum daily air temperature assuming an average snow density of 250 kg/m^2. The maximum state of internal energy is taken as zero and it is assumed that no melt water is released by the snowcover until it reaches its maximum state. An algorithm that accounts for internal energy changes, the liquid and frozen water content of a snowcover and the amount of snowcover runoff is described.

The dates snowcover runoff "started" and "ended", predicted by the EBSM, are compared with observations of the time-depletion in snowcover depth at Bad Lake and Regina over a number of years. Similar comparisons are also presented between the "start" of simulated runoff and observed flow from the Davin (area = ~10 km^2) and Wascana Creek (area = ~350 km^2) watersheds in south-central Saskatchewan near Regina. Reasonable agreement is shown between the time elements of simulated and observed data; however, the results of the analysis point to the need for the development of routing routines to account for the effects of storage on the translation and attenuation of melt quantities through a snowcover and in snow-filled gullies. The latter is particularly important for simulations in low snow years.

The EBSM is incorporated into the U.S. Corps of Engineers Streamflow Synthesis and Reservoir Regulation System (SSARR) and the system used to simulate streamflow from snowmelt on the Creighton Tributary (area ~11 km^2) and the Wascana Creek watershed (area ~350 km^2) in Saskatchewan. Simulations for the same years with SSARR, using the degree-day method to calculate melt rates, are also given. It is demonstrated that the EBSM is workable and when incorporated in an operational forecasting system will produce estimates of streamflow from snowmelt of *at least* equal accuracy to those obtained by the degree-day method.

The limitations of the EBSM for calculating runoff quantities are emphasized.

6. REFERENCES CITED

Baier, W. and G.W. Robertson. 1965. Estimation of latent evaporation from simple weather observations. Canadian Journal of Plant Science 45:276-284.

Brunt, D. 1932. Notes on radiation in the atmosphere. Quarterly Journal of the Royal Meteorological Society 58:389-420.

Brutsaert, W. 1982. Evaporation into the Atmosphere. D. Reidel Publishing Company, London, England. 299 pp.

Davies, J.A. 1965. The use of Gunn-Bellani distillator to determine net radiative flux for West Africa. Journal of Applied Meteorology 4:547-549.

Davies, J.A. 1967. A note on the relationship between net radiation and solar radiation. Quarterly Journal of the Royal Meteorological Society 93:109-115.

Davies, J.A. and D.H. Buttimor. 1969. Reflection coefficients and net radiation at Simcoe, Southern Ontario. Agricultural Meteorology 6:373-386.

Davies, J.A. and S.B. Idso. 1979. Estimating the surface radiation balance and its components. In Modification of the Aerial Environments of Crops (B.J. Barfield and J.F. Gerber, eds.). American Society of Agricultural Engineers, St. Joseph, MO. pp. 183-210.

de Jong, B. 1973. Net Radiation Received by a Horizontal Surface at the Earth. Delft University Press, Rotterdam, The Netherlands. 51 pp.

Dybvig, W.L. 1977. The computer simulation of mass and heat transfer in a one-dimensional snowpack. Saskatoon, SK: Univeristy of Saskatchewan. 148 pp. M.Sc. Thesis.

Erickson, D.E.L., W. Lin and H. Steppuhn. 1978. Indices for estimating prairie runoff from snowmelt. Paper presented to Seventh Symposium of Water Studies Institute, Applied Prairie Hydrology, Saskatoon, Sask.

Garnier, B.J. and A. Ohmura. 1970. The evaluation of surface variations in solar radiation income. Solar Energy 13:21-34.

Gates, D.M. 1980. Biophysical Ecology. Springer-Verlag, New York, NY. 611 pp.

Granger, R.J. 1977. Energy exchange during melt of a Prairie snowcover. Saskatoon, SK: University of Saskatchewan. 122 pp. M.Sc. Thesis.

Granger, R.J. and D.H. Male. 1978. Melting of a prairie snowpack. Journal of Applied Meteorology 17(12):1833-1842.

Granger, R.J., D.H. Male and D.M. Gray. 1978. Prairie snowmelt. Proceedings of Applied Prairie Hydrology Symposium, Saskatoon, SK., Seventh Symposium of Water Studies Institute, Saskatoon, SK.

Gray, D.M. and P.G. Landine. 1985. Modelling snowmelt infiltration to frozen Prairie soils. Unpublished Report prepared for Research Management Division, Alberta Environment, Edmonton under RMD.83-34A, AE Contract No. 85-0569, 118 pp.

Gray, D.M., J.W. Pomeroy and P.G. Landine. 1986. Development and performance evaluation of energy balance snowmelt models. Unpublished Report prepared for Research Management Division, Alberta Environment, Edmonton, under RMD.83-34B, AE Contract No. 86-0826, 67 pp.

Hicks, B.B. and H.C. Martin. 1972. Atmospheric turbulent fluxes over snow. Boundary-Layer Meteorology 2:496-502.

Kondratyev, K. Ya. 1969. Radiation in the Atmosphere. International Geophysical Series, Academic Press, New York, NY. Volume 12: 912 pp.

Kuz'min, P.P. 1972. Melting of Snow Cover. Israel Program of Scientific Translations, Jerusalem, Israel. 290 pp.

List, R.J. 1968. Smithsonian Meteorological Tables. 6th Edition. The Smithsonian Institute, Washington, DC. 527 pp.

Male, D.H. and D.M. Gray. 1975. Problems in developing a physically based snowmelt model. Canadian Journal of Civil Engineering 2(4):474-488.

Male, D.H. and D.M. Gray. 1981. Snowcover ablation and runoff. In Handbook of Snow: Principles, Processes, Management and Use (D.M. Gray and D.H. Male, eds.). Pergamon Press Canada Limited, Toronto, ON. pp. 360-436.

Male, D.H. and R.J. Granger. 1979. Energy mass fluxes at the snow surface in a Prairie environment. Proceedings of Modelling Snowcover Runoff (S.C. Colbeck and M. Ray, eds.). U.S. Army Cole Regions Research and Engineering Laboratory, Hanover, nh. pp. 101-124.

Male, D.H. and R.J. Granger, 1981. Snow surface energy exchange. Water Resources Research 17(3):609-627.

Mateer, C.L. 1955. A preliminary estimate of average insolation in Canada. Canadian Journal of Agricultural Science 35:579-594.

Mudiare, O. 1985. Influence of light rainfall activity and cloud cover on evapotranspiration demands. Saskatoon, SK: University of Saskatchewan. 105 pp. Ph.D. Thesis.

McKay, G.A. 1964. Relationships between snow survey and climatological measurements for the Canadian Great Plains. Proceedings of the 32nd Annual Meeting of the Western Snow Conference, April 21-23, 1964, Nelson, BC. pp.9-18.

Nash, J.E. and J.V. Sutcliffe. 1970. River flow forecasting through conceptual models. Journal of Hydrology, 10:282.

O'Neill, A.D.J. 1972. The energetics of shallow prairie snowcovers. Saskatoon, SK: University of Saskatchewan. 197 pp. Ph.D. Thesis.

Penman, H.L. 1948. Natural evaporation from open water, bare soil and grass. Proceedings of the Royal Society A193:120-145.

Satterlund, D.R. 1979. An improved equation for estimating long-wave radiation from the atmosphere. Water Resources Research 15:1643-1650.

U.S. Army Corps of Engineers. 1972. Program description and user manual for SSARR model, Program 724-KJ-Goolo. U.S. Army Corps of Engineers, North Pacific Division, Portland, OR.

N.L.C. - B.N.C.
3 3286 08536117 4